J. Vis. Commun. Image R. 81 (2021) 103333

Contents lists available at ScienceDirect

J. Vis. Commun. Image R.

journal homepage: www.elsevier.com/locate/jvci

Full length article

Improving UNIWARD distortion function via isotropic construction and hierarchical merging☆

Qingxiao Guan [a], Hefeng Chen [a,*], Weiming Zhang [b,*], Nenghai Yu [b]

[a] Computer Engineering College, Jimei University, Xiamen, 361021, China
[b] CAS Key Laboratory of Electromagnetic Space Information, University of Science and Technology of China, Hefei 230026, China

ARTICLE INFO

MSC:
41A05
41A10
65D05
65D17

Keywords:
Steganography
Distortion
UNIWARD

ABSTRACT

Distortion function is designed for evaluating the cost of modifications in adaptive steganography. UNIWARD is a successful and popular distortion scheme which achieves high performance both for spatial and JPEG images. In this paper, we analyze the UNIWARD scheme with some empirical rules of distortion function designation. Based on that we propose our scheme to improve UNIWARD distortion. In our scheme, we focus on the symmetric characteristic of UNIWARD, and suggest that not only use original wavelet filters but also their flippings to calculate sub-models of UNIWARD distortion to maintain its isotropic properties. Moreover, we design several schemes to merge sub-models, which could maintain its invariance regard to flipping or rotation and improve its security against steganalysis detection. Experimental results show our revised UNIWARD achieves better performance for spatial and JPEG image in comparison with original UNIWARD.

1. Introduction

Modern adaptive image steganography is built on distortion function scheme and syndrome-trellis codes (STCs) [1]. Distortion function is specifically designed to calculated cost values from content of image. It assigns cost values to each pixel or DCT coefficient as a measurement of the distortion caused by modifying it in embedding. STCs ensures that the message been correctly embedded in cover image meanwhile the sum of cost aroused by modifications been minimized. It is proved in many experiments that embedding efficiency of STCs approximates the theoretic ideal bound deduced from payload limited scheme(PLS) theory [1]. Therefor STCs is almost an ideal implementation of PLS embedding and consequently the research interest are mostly concentrate in designing distortion function schemes.

Distortion function sets a goal of making the modification in embedding occurs in secure areas thus reduce its statistical disturbance which may captured by steganalysis methods [2–10]. It greatly dominates the security of adaptive steganography. In early stage, the first two distortion function schemes HUGO [11] and WOW [12] are proposed for spatial image. They use filters, either differencing or wavelet, to reflect the edge or texture of image content. This basic idea are inherited by many following distortion schemes. Holub et al. made a breakthrough in distortion function by a wavelet based construction, which is known as UNIWARD distortion [13]. UNIWARD uses wavelet transformation on spatial data of image, and calculates the modification impact to wavelet coefficients. Based on this idea, two versions of UNIWARD, S-UNIWARD and J-UNIWARD, are derived respectively for spatial image [14] and JPEG image. In recent years, many distortion schemes have been proposed. Li et al. present two rules for designing spatial distortion function in [15], which are "complexity the first" and "spread the second". Guided by these two rules, HILL distortion uses a high pass filter and two low pass filters in distortion function, and made a remarkable progress. Ni et al. proposed UERD [16] for JPEG image. The idea of UERD is different from J-UNIWARD, it directly utilizes the information in DCT domain and considers both inter and intra block information. UERD is advanced by Su et al. and result in Generalized Uniform Embedding Distortion(GUED) [17] scheme. GUED joints wavelet impaction, Gabor filter residuals, and UERD together, and it takes advantages when payload rate is higher. Above described distortion functions belong to handicraft designed schemes. Yet another way of designing distortion function has been invented by Fridrich and Sedighi, namely model driven distortion function. In contrast to the bottom-up approach of designing distortion function, methods of this kind firstly take hypothesis of optimal detector into account to obtain the proper modification probabilities, and then according to PLS theory, they are converted to cost values. This framework produces some high secure distortion function schemes such as MVG [18] and MiPOD [19].

Provided proposed distortion functions, some techniques are incorporated into them for some specific improvements. Wang et al.

☆ This paper has been recommended for acceptance by Zicheng Liu.

* Corresponding authors.
E-mail addresses: chenhf@jmu.edu.cn (H. Chen), zhangwm@ustc.edu.cn (W. Zhang).

https://doi.org/10.1016/j.jvcir.2021.103333
Received 7 December 2020; Received in revised form 29 August 2021; Accepted 25 September 2021
Available online 5 October 2021
1047-3203/© 2021 Published by Elsevier Inc.

proposed to estimate the uncompressed image from compressed JPEG cover image as a reference by wiener filter, and modulate the distortion costs with side-information to resist detection from certain steganalysis feature [20]. This method could largely increase its undetectability when the targeted steganalysis feature is known to steganographer. Besides works on designing distortion function schemes, Zhou et al. proposed Controversial Pixel Prior(CPP) [21][22] to assemble different distortions to improve security. This ensemble method can make use of already existing distortion functions for a better ensemble one. CPP is effective to combine distortion functions from different principle but with similar performance. In Section 5, we also discuss the difference in usage between CPP and our method.

Distortion function plays as a key role for steganography in resisting feature based or deep model based steganalysis, and they also provide premise for none-additive distortion schemes. In this paper, we investigate the revision of S-UNIWARD and J-UNIWARD since they are similar in principles, and for following reasons:

1. J-UNIWARD is so far one of the most successful distortion function for JPEG steganography. It is not only a high secure scheme for ordinary JPEG steganographic embedding but also an excellent distortion function for robust JPEG steganography [23][24][25][26][27] to resist JPEG recompression, which can achieve high robustness and security while reducing the payload expense for error correction bits. Therefore, improving J-UNIWARD is important.
2. For spatial images, although some latest distortion schemes, such as HILL [15] or MiPOD [19] et al., could gain better security performance for most cases, S-UNIWARD still take its advantages for some kinds of images, such as on spatial images of original size and with acquisition noise [28]. These kinds of image data are also very common in real application environments. Besides, some recently proposed none-additive distortion schemes adopt S-UNIWARD as its basis [29]. Hence, an improvement on S-UNIWARD has practical significance.
3. Sub-models of UNIWARD expanded in this work are calculated by the same procedure with wavelet in different directions. Namely, they are homogeneous sub-models. However, to the best of our knowledge, there are no work specifically focus on merging distortion sub-models of homogeneity, so it needs more studying.
4. As a state-of-the-art spatial distortion, UNIWARD can collaborate with other distortions functions via CPP ensemble strategy and yield more powerful distortion schemes. Moreover, UNIWARD could provide diversified ingredients for ensemble models by using abundant wavelet filters.

Above reasons reveals our motivation of research work on UNIWARD. Both S-UNIWARD and J-UNIWARD uses 3 bands of wavelet coefficient to obtain 3 sub-models of distortion function, and then sum up them as the result. In fact, the original UNIWARD scheme only considered the completeness of bands of wavelet, but ignored some symmetric properties. For this reason, it seems somehow biased and unnatural. We solve this problem by adding more sub-models to encompass all directions and consequently makes it symmetric. Although this simple strategy of revising UNIWARD could solve the aforementioned problem, we argue that there are more room for improvement by innovation new methods for merging these sub-models with different bands and directions, rather than merely adding up them as is in original UNIWARD. Therefor we design several merging method in this paper. The contributions of this paper are list as follow:

1. We investigate the symmetric properties of cost scheme and analyze the defect in construction of UNIWARD due to the asymmetry of db wavelet, and an exhaustive experimental testing of UNIWARD with regard to db wavelet are presented in this paper.
2. We propose revised UNIWARD distortion scheme by calculating sub-models using wavelet filters and their symmetric versions to reflect the local complexity via different combination of directions. Compare to the original UNIWARD, proposed revised UNIWARD is more secure and plausible.
3. With sub-models of UNIWARD, we further explore the new method for merging them, and a hierarchical strategy is proposed. We compare several implementation of merging method and analyze them. We notice that some other distortion function schemes follows similar principles as UNIWARD, and merging method proposed in this paper can be applied to them without obstacle.

To verify the necessity of using db wavelet, we also tried to replacing db wavelet with some other symmetric filters in constructing UNIWARD, which are discussed in Section 5. Unfortunately, their performances are poor and thus we turn back to db wavelet as is advocated by Holub in [13]. Another alternative of db wavelet is Gabor filter bank with different directions, scales, and phases. Gabor filters have been successfully utilized by steganalysis feature GFR, and it also gives comparable results for some distortion function schemes [5]. However, they requires using much more filters than db filters in UNIWARD. Besides, unlike db wavelet, Gabor filters are inseparable and hence result in much more computational burden in convolution. These makes UNIWARD distortion more popular, especially for JPEG images and on resource limited platform such as mobile devices. So we focus on it in this paper for its practicality and popularity. However, methods of this work are not only applicable to it but also to other distortion functions.

The rest of this paper is organized as follow: Section 2 is preliminaries of this paper, we define notations used in this paper and give a brief review of original UNIWARD in this section. And characteristics of distortion function, which elicits some ideas of this work, are also described in it. Section 3 is the main part of this paper, in which we propose our method and make a discussion about it. Experimental results are presented in Section 4. In Section 5, we discuss several issues of this work. Finally, we draw a conclusion in Section 6.

2. Preliminaries

2.1. Notations

A symbol in boldface of uppercase is a matrix or a vector. For example, in this paper, spatial pixel data array of a image is wrote as $\mathbf{X}$, and the cost image is $\mathbf{C}$. Also, the wavelet filters of high band and low band are vectors $\mathbf{H}$ and $\mathbf{L}$. The letter of lowercase is the scalar which could be an index in subscript, or an elements in a matrix or vector. For example $x_{i,j}$ is the value of the pixel in location (i, j) in image $\mathbf{X}$. Besides, we shall define another kind of scalar notation which is letter of uppercase for the size of matrices, vectors or sets. For example, a matrix $\mathbf{X}$ of size $M \times N$ can be written as $\mathbf{X} \in \Re^{M \times N}$.

Matrix functions $|\mathbf{X}|$ and $1\backslash\mathbf{X}$ respectively take the absolute value and the reciprocal value of each elements in matrix $\mathbf{X}$. In addition, a letter or a word in italics is a function which receives one or more matrices as variable and output a resultant matrix. There are several functions that will be mentioned in next sections:

$fliplr(\cdot)$ and $flipud(\cdot)$ are flipping functions which flip matrix horizontally and vertically. $rot90(\cdot)$, $rot180(\cdot)$ and $rot270(\cdot)$ are rotation functions which rotate matrix 90, 180 and 270 degrees clockwise. Besides, in this paper, two important functions $max(\cdot)$ and $min(\cdot)$ are used in designing merging strategy. Respectively they receive multiple matrices of the same size as input, and return a matrix containing max or min values of elements in each position of input matrices.

For convenience, we define the flipping of a vector by putting superscript of symbol prime on it. So the flipping of wavelet filters $\mathbf{H}$ and $\mathbf{L}$ are defined as $\mathbf{H}'$ and $\mathbf{L}'$:

$$\mathbf{H}' = fliplr(\mathbf{H}), \mathbf{L}' = fliplr(\mathbf{L}) \tag{1}$$

In fact, $\mathbf{H}'$ and $\mathbf{L}'$ have the same length of $\mathbf{H}$ and $\mathbf{L}$, but the order of their elements are reversed. In many papers, 2D wavelet filters of 3 band are denoted as **LH**, **HL** and **HH**. We inherit this notation and it is also valid for $\mathbf{H}'$ and $\mathbf{L}'$ in this paper. For example, $\mathbf{L}'\mathbf{H}$ indicates a matrix which is formulated by multiplying transpose of $\mathbf{L}'$ with $\mathbf{H}$.

A calligraphy letter denote a set containing matrices or several subsets, and the elements in it can be specified by using brace $\{\cdot\}$. For example, set $\mathcal{W} = \{\mathbf{LH}, \mathbf{HL}, \mathbf{HH}\}$ contains 3 wavelet filters.

Convolution is a key step in UNIWARD. We define the fully convolution of matrix $\mathbf{X}$ and matrix $\mathbf{Y}$ as $\mathbf{X} \otimes \mathbf{Y}$.

2.2. Characteristic of distortion functions

Distortion functions aim to evaluate the cost of modification. Empirically, modifying pixels or coefficients in areas of complex texture or sharp edge areas are more secure than that in smooth content area. This rule is summarized by Li et al. as "complexity the first", and almost all the distortion functions abide by it. We notice that although distortion function schemes are composed by a serial of procedures, they are all carried out locally in the image for each cost value. This is understandable since the distortion function evaluates pixels' or coefficients' fitness of modification according to image content around it. And it suggest that the whole process of calculating a cost value only depend on a local area in the image.

A general form of distortion function can be described as a function of calculating the cost value of a pixel (or DCT coefficient) $x_{i,j}$ from a subimage $\mathbf{N}_{i,j}$ containing its neighboring pixels:

$$dist : \Re^{M\times M} \rightarrow \Re \tag{2}$$

where M is the size of subimage. For example, S-UNIWARD use db8 wavelet whose length is 16, so we can figure out that $M = 31$ due to two convolutional operations in calculating S-UNIWARD(see (3) in Section 2.3).

Function *dist* reflects the connection between local information of a subimage $\mathbf{N}_{i,j}$ and cost value $\rho_{i,j}$ for pixel(or coefficient) in coordinate (i, j). From this point, we argue that it is desirable to ensure that *distortion* being invariant to flipping and rotating 90, 180 and 270 degree operation on $\mathbf{N}_{i,j}$, because these operations do not change the local information of $\mathbf{N}_{i,j}$, i.e. the relationship between central pixel $x_{i,j}$ and its neighboring pixels in $\mathbf{N}_{i,j}$ is the same after flipping or rotating $\mathbf{N}_{i,j}$. This rule is intuitive but obviously sound, since we expect that if an image has been flipped or rotated 90, 180 or 270 degree, the cost value of each pixel be the same as their counterparts in original image. In this paper we call this rule "isotropic construction". Actually, some proposed distortion function schemes, such as HILL, MiPOD and UERD, already conform to this rule, but UNIWARD does not. The purpose of emphasizing it is twofold. Firstly, it implicitly requires that any directional procedure in distortion function construction must be guarantee to be applied for all directions. For example, if an asymmetric filter is used in constructing distortion function, typically we have to use its flippings and rotations as well to keep the result isotropic. This step is the premise of "isotropic construction". Secondly, merging method for cost values calculated from directions should keep the result invariant to rotation and flipping. Actually, guided by this rule, in this paper we propose several hierarchical merging methods.

These rules are designed in terms of direction properties, and they are for merging distortion schemes in directional operations. In this paper, we designed hierarchical merging methods, and each of them includes a phase of directional cost merging which meets this requirement.

2.3. Brief review of UNIWARD distortion scheme

In this section we give a brief review of UNIWARD proposed in [13], and we name it "original UNIWARD" in this paper to avoid any confusion. As aforementioned, original UNIWARD includes two versions, S-UNIWARD and J-UNIWARD for spatial image and JPEG image respectively. They are respectively designed for spatial and JPEG image formats based on the same principle. Rather than rephrasing original UNIWARD which appeared in many papers, we reveal its implementation details more clear in our defined notation to make readers aware its problem and understand our work. At first, we begin with S-UNIWARD. The whole process of S-UNIWARD can be recaped as:

$$\sum_{\mathbf{F}\in\mathcal{W}} (1 \setminus (|\mathbf{X} \otimes \mathbf{F}| + \varepsilon)) \otimes rot180(|\mathbf{F}|) \tag{3}$$

where $\mathbf{X}$ is the spatial image, $\mathcal{W} = \{\mathbf{LH}, \mathbf{HL}, \mathbf{HH}\}$ and ε is a small positive value for avoiding dividing by zero. Formula (3) is sum of 3 sub-models of cost. Each sub-model are obtained by two steps. The first step $1 \setminus (|\mathbf{X} \otimes \mathbf{F}| + \varepsilon)$ is evaluating the complexity of image contents by wavelet filter $\mathbf{F}$, and the second step is calculating impaction on them by convolving it with $rot180(|\mathbf{F}|)$. J-UNIWARD differs from S-UNIWARD only in their ways of calculating impaction. In J-UNIWARD, for DCT coefficient of frequency (a, b) in DCT block (i, j), it crops a submatrix of size 23×23 centered in block (i, j) from matrix $1 \setminus (|\mathbf{X} \otimes \mathbf{F}| + \varepsilon)$, then take its hadamard product with a mask $|\mathbf{F} \otimes \mathbf{DCT}_{a,b}|, \mathbf{F} \in \mathcal{W}$, and sum elements up as the cost value. Where $\mathbf{DCT}_{a,b}$ is 2D DCT base of frequency (a, b).

From above description, we can clear see that both S-UNIWARD and J-UNIWARD do not take any measure to symmetrize the distortion function. Hence due to the asymmetric of wavelet filter $\mathbf{L}$ and $\mathbf{H}$, original UNIWARD do not comply with the rule proposed in Section 2.2.

3. Revising UNIWARD distortion function scheme

In this section we present our schemes of revising UNIWARD scheme which includes two steps. The first step is calculating the sub-models of cost, and the second is merging them.

3.1. Isotropic submodels

As we discussed in Section 2.3, the original UNIWARD only adopt standard wavelet filters. Although in wavelet decomposition these 3 filters are sufficient to preserve information in wavelet bands and reconstruct the image, nevertheless, considering the difference of wavelet's utilities in steganographic distortion function and wavelet decomposition, in fact they are insufficient for UNIWARD. For each wavelet filter of a band, it may evaluates pixels' (or coefficients') "security" partially in one direction, but neglects their defect in other directions. As we known, many powerful steganalysis schemes usually extract feature by residuals and coocurrence matrices in symmetric directions [5,8,30–33], thus this distortion function scheme in biased direction somehow may leave some artifacts.

For this problem, we calculate more sub-models of UNIWARD not only by wavelet filters used in original UNIWARD: $\mathcal{W} = \{\mathbf{LH}, \mathbf{HL}, \mathbf{HH}\}$, but also their flippings: $\{\mathbf{L}'\mathbf{H}, \mathbf{L}\mathbf{H}', \mathbf{L}'\mathbf{H}', \mathbf{H}'\mathbf{L}, \mathbf{H}\mathbf{L}', \mathbf{H}'\mathbf{L}', \mathbf{H}'\mathbf{H}, \mathbf{H}\mathbf{H}', \mathbf{H}'\mathbf{H}'\}$. We denote the set containing these 12 wavelet filters as $\mathcal{W}'$ in which the elements correspond to 12 sub-models of cost. These sub-models are calculated by the same procedure as in original UNIWARD. Fig. 1 shows the modification probabilities of original S-UNIWARD and revised S-UNIWARD with the same merging strategy in original UNIWARD. Revised S-UNIWARD in Fig. 1(c) is the simplest extension of original S-UNIWARD, from which we can see that original S-UNIWARD exhibits more directional inconsistency in certain direction, while revised S-UNIWARD is smoother in all directions than original S-UNIWARD.

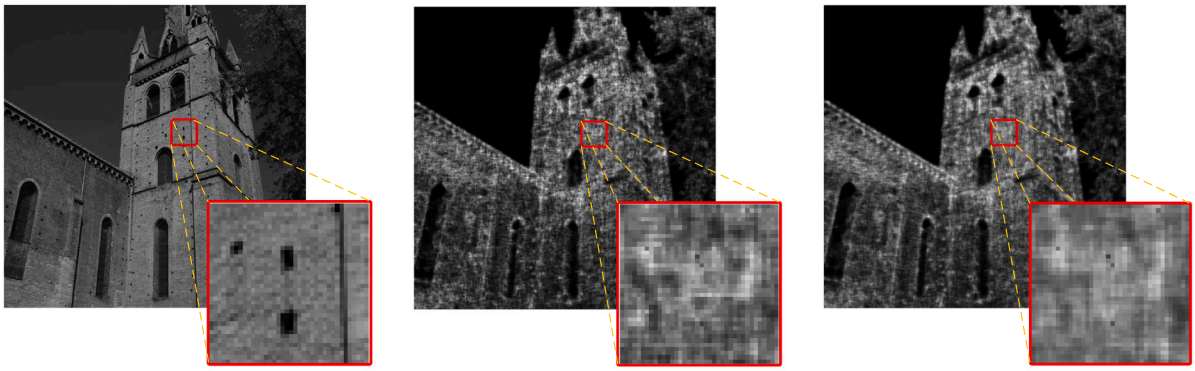

(a) 5199.pgm (b) original S-UNIWARD (c) revised S-UNIWARD

Fig. 1. Modification probability of original S-UNIWARD and revised S-UNIWARD by using wavelets in all directions with 0.4 bpp payload rate. (a) is image 5199.pgm in BOSSv1.01 image set. (b) is Modification probability of original S-UNIWARD. (c) is Modification probability of revised S-UNIWARD by using filters in $\mathcal{W}'$ and the same merging methods as in original S-UNIWARD. We suggest readers to zoom in this figure to compare details of (b) and (c).

For the convenience in next subsection, we define 3 partitions of the set $\mathcal{W}'$ respectively according to bands and directions of filters. The first one $\mathcal{B} = \{\mathcal{B}_1, \mathcal{B}_2, \mathcal{B}_3\}$ is a partition according to bands:

$$\mathcal{B}_1 = \{\mathbf{LH}, \mathbf{L'H}, \mathbf{LH'}, \mathbf{L'H'}\} \tag{4}$$

$$\mathcal{B}_2 = \{\mathbf{HL}, \mathbf{H'L}, \mathbf{HL'}, \mathbf{H'L'}\} \tag{5}$$

$$\mathcal{B}_3 = \{\mathbf{HH}, \mathbf{H'H}, \mathbf{HH'}, \mathbf{H'H'}\} \tag{6}$$

Each element in $\mathcal{B}$ is a subset containing wavelet filter of a band and its flipping. Take $\mathcal{B}_1$ as example, $\mathbf{LH} = flipud(\mathbf{L'H}) = fliplr(\mathbf{LH'}) = flipud(fliplr(\mathbf{L'H'}))$, and this is similar for filters in $\mathcal{B}_2$ and $\mathcal{B}_3$.

The second partition $\mathcal{D} = \{\mathcal{D}_1, \mathcal{D}_2, \mathcal{D}_3, \mathcal{D}_4\}$ is in accordance with directions:

$$\mathcal{D}_1 = \{\mathbf{LH}, \mathbf{HL}, \mathbf{HH}\} \tag{7}$$

$$\mathcal{D}_2 = \{\mathbf{L'H}, \mathbf{H'L}, \mathbf{H'H}\} \tag{8}$$

$$\mathcal{D}_3 = \{\mathbf{LH'}, \mathbf{HL'}, \mathbf{HH'}\} \tag{9}$$

$$\mathcal{D}_4 = \{\mathbf{L'H'}, \mathbf{H'L'}, \mathbf{H'H'}\} \tag{10}$$

Each element in $\mathcal{D}$ is a set containing wavelet filters flipped from standard wavelet of 3 bands. In fact, $\mathcal{D}_1$ contains the standard wavelet filters utilized by the original UNIWARD. Filters in $\mathcal{D}_2$, $\mathcal{D}_3$ and $\mathcal{D}_4$ are generated by respectively applying $rot180(\cdot)$, $rot90(\cdot)$ and $rot270(\cdot)$ on filters in $\mathcal{D}_1$.

Next we introduce the third partition which is a variation of the second one. By observing the quantity of elements in filters **LH**, **HL** and **HH** (see Fig. 2), we can find that their major magnitudes mainly distribute in left-down, right-up and left-up respectively. This implies that in original UNIWARD, filters of 3 bands are "scattered" in 3 different directions. From this point, we reorganize the partition $\mathcal{D}$ and yield a new partition $\mathcal{D}^* = \{\mathcal{D}_1^*, \mathcal{D}_2^*, \mathcal{D}_3^*, \mathcal{D}_4^*\}$ that each element in it is a subset containing wavelets filters of 3 band in the same direction.

$$\mathcal{D}_1^* = \{\mathbf{LH}, \mathbf{H'L'}, \mathbf{H'H}\} \tag{11}$$

$$\mathcal{D}_2^* = \{\mathbf{L'H}, \mathbf{HL'}, \mathbf{HH}\} \tag{12}$$

$$\mathcal{D}_3^* = \{\mathbf{LH'}, \mathbf{H'L}, \mathbf{H'H'}\} \tag{13}$$

$$\mathcal{D}_4^* = \{\mathbf{L'H'}, \mathbf{HL}, \mathbf{HH'}\} \tag{14}$$

By these 3 partitions, we introduce a concept of "homogeneous sub-models", which is a set of cost sub-models calculated by the certain kind of filters isotropically constructed in different symmetric directions with regard to flipping or rotation. For example, sub-models calculated by filters in $\mathcal{B}_1$ are homogeneous distortion sub-models because they are obtained by filter **LH** and its flipping and rotation, and also the sub-models from elements in $\mathcal{D}$ or $\mathcal{D}^*$.

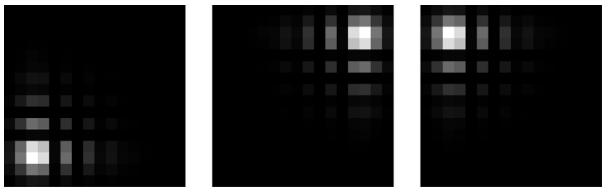

(a) **|LH|** (b) **|HL|** (c) **|HH|**

Fig. 2. Magnitude of db8 wavelet filters of band **LH**, **HL** and **HH**. Grids with lighter color are elements of larger quantity.

3.2. Hierarchical merging schemes

The wavelet filters in the original UNIWARD only refer to properties of bands, thus its merging methods is quite simple. However in our work, filters have two different properties: band and direction, so we tentatively designed more advisable merging methods to investigate if it is possible to enhance the performance. Meanwhile, we stick to simplify and interpretability in designing thus they are easy to be understood and implemented.

Our proposed merging methods include two phases in which merging operation functions are denoted as $merge1$ and $merge2$. Given a partition of set $\mathcal{W}'$: $\mathcal{S} = \{\mathcal{S}_1, \mathcal{S}_2, \ldots \mathcal{S}_K\}, \bigcup_i \mathcal{S}_i = \mathcal{W}', \mathcal{S}_i \bigcap \mathcal{S}_j = \emptyset, i \neq j$, submodels calculated by filters in $\mathcal{S}_i$ are merged in the first phase by $merge1$, i.e. $merge1$ is applied to each subset $\mathcal{S}_i, i = 1, \ldots, K$, and thus result in newly generated K submodels $\mathbf{C}_i, i = 1, 2 \ldots K$. In the second phase, $\mathbf{C}_i, i = 1, 2 \ldots K$ are merged by $merge2$ to the final result: $\mathbf{C} = merge2(\mathbf{C}_1, \mathbf{C}_2 \ldots \mathbf{C}_K)$. Our merging method is shown in Fig. 3.

Based on previous definitions, a merging scheme can be specified by a triplet $(\mathcal{S}, merge1, merge2)$. The motivation of designing hierarchical merging is that we can use different merging methods for directions and bands. The merging method in original UNIWARD is simply summing up sub-models of different bands. This method can be applied to both phases in hierarchical merging, and we denote it as "+ ". Besides, two merging methods max and min, which are already defined in Section 2.1, are used for merging isotropically constructed sub-models according to directions. The whole merging schemes are produced by different combinations of these 3 merging functions in two phases. Now we present all our merging schemes by $\mathcal{B}$, $\mathcal{D}$ defined in previous Section 3.1 as follow:

$$Scheme1 : (\mathcal{B}, +, +) \tag{15}$$

$$Scheme2 : (\mathcal{B}, max, +) \tag{16}$$

$$Scheme3 : (\mathcal{B}, min, +) \tag{17}$$

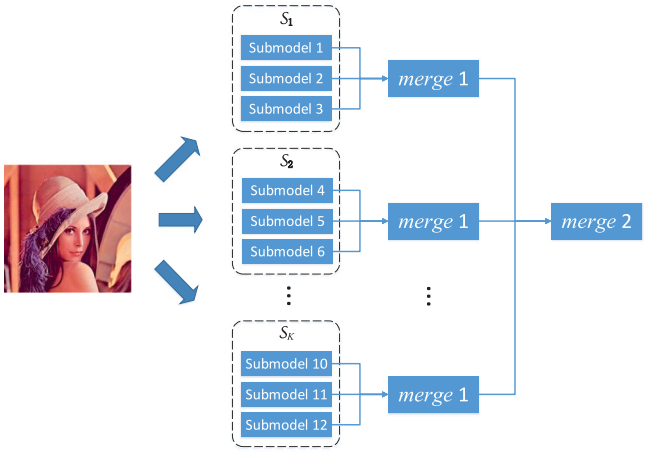

Fig. 3. Hierarchical merging strategy.

$$Scheme4 : (D, +, max) \tag{18}$$

$$Scheme5 : (D, +, min) \tag{19}$$

$$Scheme6 : (D^*, +, max) \tag{20}$$

$$Scheme7 : (D^*, +, min) \tag{21}$$

Scheme 1–7 are applied to both revised S-UNIWARD and J-UNIWARD. Scheme 1 is a straightforward extension of original UNIWARD by isotropic construction. In addition, for spatial images we design another scheme, scheme8: $(\mathcal{B}', max, +)$, where $\mathcal{B}' = \{\mathcal{B}_1 \cup \mathcal{B}_2, \mathcal{B}_3\}$. It is designed with the consideration that for spatial images, the vertical and horizontal direction can be treated identically. This philosophy is also embodied in many steganalysis feature [8]. Actually we also tested the counterpart of scheme8: $(\mathcal{B}', min, +)$, but its performance is not good in all the experiments, so we omit it in this paper.

Merging methods *max* and *min* are only applied for homogeneous sub-models, because these sub-models only differs in directions, which means they are comparable. Merging method *max* can be explained as a conservative method which determines the cost value of a pixel or coefficient by sub-models in "the least secure" direction, thus the security of it is evaluated by its "shortest barrel wood". While *min* is an aggressive method which only makes use of "the most secure" direction and takes the risks of ignoring others. Comparing to them, method "+" is a moderate one.

it is obvious that Scheme 1–7 complies to rules presented in Section 2.2. And these schemes are so simple that they would not bring too much extra computational afford in merging.

4. Experimental results

4.1. Setup

Our experiments includes three parts. The first two part are tested on BOSSbase V1.01[34] to compare the performance of revised UNIWARD with that of original UNIWARD for spatial and JPEG image respectively. BOSSbase V1.01[34] contains 10000 512×512 gray-scales images. The security performances of these two parts is evaluated by state-of-art steganalysis feature and ensemble FLD classifier [35]. Stego image set are generated by simulating steganographic embedding on covers. 5000 pairs of cover/stego images randomly selected from cover set and stego set are used as training samples, and 5000 pairs are left for testing. In each experiment, we repeat this procedure 10 times using different rand seed to randomly splitting image set into training/testing set. Therefore we can calculate the mean value and deviate of 10 results. In order to test the significance of improvement. we also implement t-test on experimental results respect to original UNIWARD, and we set significance level for the test to 0.05. The experimental results of this paper are presented in tables in which the underlined results are best results for each payload rate and wavelet type, and results in boldface are best ones for each payload rate over all wavelet types. The results with statistic importance is denoted with an asterisk "*".

The third part is tested on a larger dataset ALASKA2 [36] with recently developed deep model Efficient Net. ALASKA2 includes 80000 images which is sufficient for training deep network. Specifically, we use ALASKA2 of size 256×256.

Experiments are carried out on different payload rates is measured in bpp(bit-per-pixel) for spatial image and bpnz(bit per non-zero AC coefficient) for JPEG image. Performance is measured by classification error rate $P_E = \min_{P_{FA}}(P_{FA} + P_{MD})/2$ where P_{FA} is false-alarm rate and P_{MD} is miss-detection rate. P_E indicates the indistinguishability between cover images and stego images, so higher P_E corresponds to higher security of steganography methods.

In [13], Hulob et al. tested different wavelets, and suggest that db8 wavelet filter is a desirable one for original UNIWARD. Length of wavelet filters could be different, which determines the size of the local area used in calculating cost value. Considering our methods include 10 kinds of merging schemes, and in order to give a panorama view of the relationship between wavelet filter length and merging schemes, experiments on db wavelets of different length(db8-db5) with respectively to 10 merging schemes are comprised in our experiment. Besides db wavelet, we also tested more types of wavelet filter, such as coif, sym and bior wavelet, but in most experiments their performances are no better than db wavelet. These results is coincident with Hulob et al. in [13], so we also suggest using the db wavelet in UNIWARD.

4.2. Experimental results on spatial image

In this subsection we present our experimental results of original S-UNIWARD and our revised S-UNIWARD with scheme 1–9 described in Section 3.2. Experiments in this part are carried out by 2 state-of-art steganalysis feature sets: SRM [8] and MaxSRMd2[5]. MaxSRMd2 is selection-channel aware feature scheme which makes use of prior knowledge of steganographic distortion function. It adopts the modification probability values as weights in computing co-occurrence matrices so that they could preserve more information for pixels which tend to be modified. we test our schemes and original UNIWARD on BOSS V1.01, BOSSc and BOSSc_J85 image bases. BOSSc_J85 is generated by firstly compressing images in BOSSc with Qf=85 and then decompressing them to spatial. BOSSc_J85 differs from BOSS_J85[28] because it do not resize images before compression so that acquisition noise is preserved to simulate the JPEG images directly obtained from cameras. Experiments on BOSSc and BOSSc_J85 include payload rate 0.1 bpp-0.3 bpp, and when payload rate is larger than 0.2 bpp, security of steganography on these two image is very low. As is addressed in [28], performance of WOW [12] is close to S-UNIWARD on BOSSc and it is better on BOSS_J85, so we take WOW and its revised version into comparison study on BOSSc_J85 and BOSSc. Original WOW also uses 3 wavelet filters **LH**, **HL**, **HH**. But in contrast to S-UNIWARD, it only constructs a single model. Formally, our schemes can be applied to WOW by splitting it into sub-models regard to wavelet. After some tentative experiments, we find that most of these schemes do not brings improvement to WOW as much as S-UNIWARD. So we only present the original WOW and revised WOW of scheme 1.

From Tables 1 and 2 we can see that revised S-UNIWARD on BOSS V1.01 could gain more promotion when detected by MaxSRMd2. For SRM steganalyzer, the performance of scheme 1 and scheme 3–7 are close to original S-UNIWARD, and from overall results, db5-db7 wavelet are better than db8 for S-UNIWARD. From the results on BOSS V1.01, BOSSc and BOSSc_J85, schemes with *min* are better than ones with *max*, and their performances are slightly higher than original S-UNIWARD, this implies more aggressive schemes could deliver some

Table 1
Experimental results P_E on BOSS V1.01 detected by SRM.

Wavelet	Method	Payload rate				
		0.1	0.2	0.3	0.4	0.5
db8	Original UNIWARD	40.01 ± 0.37	31.91 ± 0.44	25.87 ± 0.77	20.65 ± 0.23	16.38 ± 0.22
	Scheme 1. $(\mathcal{B},+,+)$	40.21 ± 0.26	31.95 ± 0.43	25.86 ± 0.49	20.78 ± 0.32	16.80 ± 0.41
	Scheme 2. $(\mathcal{B},max,+)$	39.64 ± 0.22	31.67 ± 0.30	25.09 ± 0.27	20.54 ± 0.27	16.13 ± 0.24
	Scheme 3. $(\mathcal{B},min,+)$	39.93 ± 0.25	31.98 ± 0.29	25.61 ± 0.20	20.75 ± 0.26	*17.11 ± 0.23
	Scheme 4. $(\mathcal{D},+,max)$	40.13 ± 0.41	31.67 ± 0.29	25.56 ± 0.23	20.62 ± 0.31	16.33 ± 0.28
	Scheme 5. $(\mathcal{D},+,min)$	40.20 ± 0.50	32.25 ± 0.24	25.78 ± 0.45	20.77 ± 0.46	16.72 ± 0.27
	Scheme 6. $(\mathcal{D}^*,+,max)$	39.92 ± 0.41	31.96 ± 0.31	25.90 ± 0.32	20.90 ± 0.37	16.41 ± 0.23
	Scheme 7. $(\mathcal{D}^*,+,min)$	40.10 ± 0.43	31.62 ± 0.21	25.58 ± 0.37	20.40 ± 0.27	16.61 ± 0.29
	Scheme 8. $(\mathcal{B}',max,+)$	39.81 ± 0.34	31.55 ± 0.25	25.59 ± 0.37	20.40 ± 0.23	16.06 ± 0.32
db7	Original UNIWARD	40.23 ± 0.31	32.29 ± 0.37	26.20 ± 0.23	20.91 ± 0.22	16.88 ± 0.29
	Scheme 1. $(\mathcal{B},+,+)$	40.32 ± 0.36	32.33 ± 0.37	26.22 ± 0.49	**21.10 ± 0.36**	16.81 ± 0.26
	Scheme 2. $(\mathcal{B},max,+)$	39.90 ± 0.42	32.02 ± 0.35	25.65 ± 0.28	20.62 ± 0.34	16.40 ± 0.45
	Scheme 3. $(\mathcal{B},min,+)$	40.34 ± 0.28	32.45 ± 0.29	26.06 ± 0.32	20.99 ± 0.26	17.01 ± 0.24
	Scheme 4. $(\mathcal{D},+,max)$	40.34 ± 0.38	32.25 ± 0.24	25.97 ± 0.29	20.71 ± 0.23	16.66 ± 0.39
	Scheme 5. $(\mathcal{D},+,min)$	**40.87 ± 0.32**	32.47 ± 0.39	26.00 ± 0.22	20.81 ± 0.31	16.96 ± 0.30
	Scheme 6. $(\mathcal{D}^*,+,max)$	40.21 ± 0.46	32.08 ± 0.37	26.12 ± 0.21	20.88 ± 0.25	16.55 ± 0.19
	Scheme 7. $(\mathcal{D}^*,+,min)$	40.16 ± 0.32	32.08 ± 0.32	26.10 ± 0.32	20.81 ± 0.33	16.90 ± 0.46
	Scheme 8. $(\mathcal{B}',max,+)$	39.77 ± 0.42	32.11 ± 0.32	25.66 ± 0.35	20.56 ± 0.37	16.35 ± 0.23
db6	Original UNIWARD	40.46 ± 0.26	32.23 ± 0.46	26.07 ± 0.28	20.91 ± 0.19	16.66 ± 0.12
	Scheme 1. $(\mathcal{B},+,+)$	40.52 ± 0.33	**32.53 ± 0.41**	26.14 ± 0.31	20.91 ± 0.34	16.69 ± 0.06
	Scheme 2. $(\mathcal{B},max,+)$	39.84 ± 0.37	31.79 ± 0.27	25.44 ± 0.24	20.52 ± 0.31	16.31 ± 0.17
	Scheme 3. $(\mathcal{B},min,+)$	40.73 ± 0.41	32.45 ± 0.27	26.23 ± 0.36	21.07 ± 0.25	16.89 ± 0.21
	Scheme 4. $(\mathcal{D},+,max)$	40.10 ± 0.29	31.82 ± 0.27	25.46 ± 0.31	20.65 ± 0.34	16.33 ± 0.31
	Scheme 5. $(\mathcal{D},+,min)$	40.69 ± 0.33	32.36 ± 0.40	26.12 ± 0.32	21.08 ± 0.30	16.79 ± 0.12
	Scheme 6. $(\mathcal{D}^*,+,max)$	40.20 ± 0.22	32.26 ± 0.34	25.71 ± 0.36	20.61 ± 0.37	16.37 ± 0.23
	Scheme 7. $(\mathcal{D}^*,+,min)$	40.48 ± 0.40	32.42 ± 0.50	26.00 ± 0.26	20.85 ± 0.34	16.75 ± 0.19
	Scheme 8. $(\mathcal{B}',max,+)$	39.87 ± 0.31	31.96 ± 0.48	25.86 ± 0.56	20.14 ± 0.18	16.63 ± 0.13
db5	Original UNIWARD	40.49 ± 0.39	32.07 ± 0.24	25.71 ± 0.41	20.61 ± 0.34	16.56 ± 0.27
	Scheme 1. $(\mathcal{B},+,+)$	40.53 ± 0.48	32.34 ± 0.30	25.70 ± 0.21	20.84 ± 0.24	16.67 ± 0.40
	Scheme 2. $(\mathcal{B},max,+)$	39.84 ± 0.40	31.53 ± 0.35	25.19 ± 0.39	19.89 ± 0.33	15.61 ± 0.23
	Scheme 3. $(\mathcal{B},min,+)$	40.70 ± 0.30	32.29 ± 0.44	**26.26 ± 0.34**	21.03 ± 0.31	16.95 ± 0.27
	Scheme 4. $(\mathcal{D},+,max)$	39.92 ± 0.33	31.72 ± 0.35	25.25 ± 0.33	20.02 ± 0.36	16.04 ± 0.28
	Scheme 5. $(\mathcal{D},+,min)$	40.51 ± 0.41	32.41 ± 0.32	26.06 ± 0.30	**21.10 ± 0.36**	16.53 ± 0.24
	Scheme 6. $(\mathcal{D}^*,+,max)$	39.99 ± 0.48	32.12 ± 0.14	25.57 ± 0.25	20.40 ± 0.25	16.17 ± 0.26
	Scheme 7. $(\mathcal{D}^*,+,min)$	40.42 ± 0.50	32.26 ± 0.24	26.02 ± 0.31	20.60 ± 0.29	16.59 ± 0.32
	Scheme 8. $(\mathcal{B}',max,+)$	39.52 ± 0.27	31.30 ± 0.44	25.13 ± 0.19	19.88 ± 0.35	15.57 ± 0.15

benefits in resist SRM detection. As we know, merging function *min* makes costs of some pixels lower, and most of these pixels located in area with pixels of low costs. So this operation, to some extend, diffuses some modification of lower costs to such adjacent pixels. On the other hand, SRM treats pixels equally, and this is why *min* is better in countering SRM.

For experimental results of MaxSRMd2 feature in Tables 2 and 4, schemes using *max* can achieve better improvement, and in most settings of experiments on BOSS V1.01, schemes using *min* are generally no better than original S-UNIWARD. This is conversely different from that of SRM. cost values of "*max*" usually means more smoothness in one direction than others. However. embedding modifications add some irregularity to these pixels, which reduces the gap between sub-models of "*max*" direction and "*min*". While MaxSRMd2 is a targeted method, this modification "misguide" MaxSRMd2 in assigning importance to pixels according to "deformed" cost values calculated in stego image. Experimental results on wavelet db8-db5 shows a consistent tendency that when payload is 0.1 bpp, scheme 2 is a good choice for MaxSRMd2, and scheme 6 outperforms other schemes with a notable margin. This result means our reorganized group of wavelet filters can concretely increasing its performance when detected by MaxSRMd2 feature (see Table 3).

From experimental results on spatial images, we can see that for both image database, db7-db5 is better than db8 in most cases, this shows that length of wavelet filter is a factor that influences the performance for spatial image steganography no matter candidate image been compressed or not. On the other hands, images in these two databases are resized with the same scale factor, so a question is that is the optimal choice of this factor invariant to resize scale? So far it is known that some research has been made on steganalysis of resized images with different resize scale and interpolation methods [37], and the distortion function for them worth more intensive research in future work.

4.3. Experimental results on JPEG image

In this subsection we present our experimental result of our revised S-UNIWARD with scheme 1–7 described in Section 3.2. Experiments in this part are carried out by GFR [3] and SCA-GFR [7]. GFR is a 17000D phase-aware feature set and is one of the most effective feature set for JPEG steganalysis. Similar to MaxSRMd2, SCA-GFR is the selection-channel-aware version of GFR. JPEG quality factor Qf is a crucial factor which greatly influence the detection results, so we test methods in Qf=95 and Qf=75. From Tables 5–7 we can see that the for both Qf=95 and Qf=75, scheme 1,3,5,7 is better than original J-UNIWARD for db6-db8. while scheme 2,4,6 are no better in most case when payload rate is larger than 0.1 bpnz. From this point, merging method *min* is suitable for JPEG homogeneous sub-models. But a interesting phenomenon shown by Table 8 that when JPEG images of Qf=75 are detected by SCA-GFR, for payload rate less than 0.3bpnz, merging method *max* is obviously better than *min*. While for 0.3bpnz payload rate, their performances are similar, and Scheme1 becomes the best one. Surprisingly this situation reversed for payload rates larger than 0.3bpnz. From these we can see that as payload rate increasing, optimal choice of merging scheme changing regularly from conservative to moderate, and finally to aggressive. As we know, correlation between contiguous JPEG blocks are more vulnerable in JPEG images with lower quality factor. When payload is small, embedding leaves relatively more artifact on inter-block than

Table 2
Experimental results P_E on BOSS V1.01 detected by MaxSRMd2.

Wavelet	Method	Payload rate				
		0.1	0.2	0.3	0.4	0.5
db8	Original UNIWARD	36.50 ± 0.35	29.04 ± 0.35	23.94 ± 0.30	19.42 ± 0.36	15.98 ± 0.33
	Scheme 1. $(\mathcal{B},+,+)$	37.16 ± 0.39	29.61 ± 0.41	23.92 ± 0.28	19.58 ± 0.34	16.28 ± 0.24
	Scheme 2. $(\mathcal{B},max,+)$	*38.00 ± 0.27	*30.45 ± 0.28	24.59 ± 0.46	20.03 ± 0.26	16.07 ± 0.36
	Scheme 3. $(\mathcal{B},min,+)$	35.16 ± 0.43	27.56 ± 0.26	22.67 ± 0.29	18.16 ± 0.30	15.10 ± 0.20
	Scheme 4. $(\mathcal{D},+,max)$	*37.49 ± 0.48	*30.04 ± 0.31	24.45 ± 0.36	19.92 ± 0.28	16.39 ± 0.30
	Scheme 5. $(\mathcal{D},+,min)$	35.65 ± 0.38	28.29 ± 0.26	22.80 ± 0.43	18.66 ± 0.22	15.48 ± 0.34
	Scheme 6. $(\mathcal{D}^*,+,max)$	*38.33 ± 0.32	*30.63 ± 0.22	*24.90 ± 0.43	20.25 ± 0.31	16.45 ± 0.33
	Scheme 7. $(\mathcal{D}^*,+,min)$	35.20 ± 0.34	27.88 ± 0.29	22.48 ± 0.33	18.08 ± 0.43	15.12 ± 0.15
	Scheme 8. $(\mathcal{B}',max,+)$	*37.61 ± 0.38	29.78 ± 0.26	24.22 ± 0.19	19.76 ± 0.35	16.09 ± 0.22
db7	Original UNIWARD	36.91 ± 0.40	29.52 ± 0.39	24.07 ± 0.21	19.80 ± 0.26	16.17 ± 0.36
	Scheme 1. $(\mathcal{B},+,+)$	37.34 ± 0.36	29.73 ± 0.36	24.36 ± 0.42	19.65 ± 0.23	16.09 ± 0.18
	Scheme 2. $(\mathcal{B},max,+)$	***38.35 ± 0.37**	*30.47 ± 0.42	24.68 ± 0.38	20.21 ± 0.42	16.45 ± 0.33
	Scheme 3. $(\mathcal{B},min,+)$	35.40 ± 0.30	28.34 ± 0.30	22.99 ± 0.41	19.02 ± 0.37	15.71 ± 0.24
	Scheme 4. $(\mathcal{D},+,max)$	37.97 ± 0.29	30.40 ± 0.45	*24.81 ± 0.28	20.11 ± 0.34	16.45 ± 0.34
	Scheme 5. $(\mathcal{D},+,min)$	36.08 ± 0.42	28.90 ± 0.24	23.46 ± 0.44	18.97 ± 0.34	15.83 ± 0.26
	Scheme 6. $(\mathcal{D}^*,+,max)$	*38.19 ± 0.37	*30.63 ± 0.43	24.98 ± 0.50	20.28 ± 0.44	16.71 ± 0.32
	Scheme 7. $(\mathcal{D}^*,+,min)$	35.75 ± 0.37	28.54 ± 0.38	22.70 ± 0.15	18.90 ± 0.43	15.22 ± 0.21
	Scheme 8. $(\mathcal{B}',max,+)$	37.79 ± 0.40	30.40 ± 0.41	24.62 ± 0.37	19.99 ± 0.28	16.37 ± 0.29
db6	Original UNIWARD	36.63 ± 0.30	29.74 ± 0.32	24.38 ± 0.45	19.82 ± 0.42	16.03 ± 0.05
	Scheme 1. $(\mathcal{B},+,+)$	37.41 ± 0.33	30.07 ± 0.42	24.64 ± 0.35	20.17 ± 0.35	16.37 ± 0.17
	Scheme 2. $(\mathcal{B},max,+)$	*38.20 ± 0.45	*30.68 ± 0.29	24.87 ± 0.34	20.39 ± 0.44	16.54 ± 0.23
	Scheme 3. $(\mathcal{B},min,+)$	35.75 ± 0.37	28.66 ± 0.51	23.49 ± 0.30	19.10 ± 0.28	15.93 ± 0.31
	Scheme 4. $(\mathcal{D},+,max)$	*37.80 ± 0.42	30.75 ± 0.41	24.68 ± 0.37	20.11 ± 0.33	16.41 ± 0.20
	Scheme 5. $(\mathcal{D},+,min)$	36.49 ± 0.49	29.27 ± 0.29	23.88 ± 0.43	19.33 ± 0.37	15.61 ± 0.19
	Scheme 6. $(\mathcal{D}^*,+,max)$	*38.07 ± 0.36	30.78 ± 0.34	25.04 ± 0.32	***20.40 ± 0.29**	16.64 ± 0.29
	Scheme 7. $(\mathcal{D}^*,+,min)$	36.00 ± 0.63	28.76 ± 0.30	23.64 ± 0.32	19.19 ± 0.23	15.43 ± 0.36
	Scheme 8. $(\mathcal{B}',max,+)$	*37.86 ± 0.24	30.51 ± 0.32	24.81 ± 0.28	20.14 ± 0.18	16.38 ± 0.19
db5	Original UNIWARD	37.15 ± 0.40	29.88 ± 0.36	24.16 ± 0.32	19.63 ± 0.28	16.20 ± 0.31
	Scheme 1. $(\mathcal{B},+,+)$	37.46 ± 0.24	30.01 ± 0.30	24.42 ± 0.41	20.06 ± 0.13	16.43 ± 0.22
	Scheme 2. $(\mathcal{B},max,+)$	*38.19 ± 0.26	***30.90 ± 0.36**	24.79 ± 0.24	20.08 ± 0.31	16.43 ± 0.32
	Scheme 3. $(\mathcal{B},min,+)$	35.65 ± 0.38	28.70 ± 0.27	23.36 ± 0.34	19.13 ± 0.44	15.80 ± 0.48
	Scheme 4. $(\mathcal{D},+,max)$	37.82 ± 0.39	30.40 ± 0.31	24.85 ± 0.32	20.11 ± 0.38	16.21 ± 0.42
	Scheme 5. $(\mathcal{D},+,min)$	36.46 ± 0.28	29.22 ± 0.46	23.68 ± 0.30	19.45 ± 0.31	16.04 ± 0.33
	Scheme 6. $(\mathcal{D}^*,+,max)$	38.03 ± 0.36	30.64 ± 0.28	***25.23 ± 0.27**	20.30 ± 0.25	***16.73 ± 0.15**
	Scheme 7. $(\mathcal{D}^*,+,min)$	35.73 ± 0.32	28.79 ± 0.49	23.52 ± 0.29	19.13 ± 0.26	15.82 ± 0.27
	Scheme 8. $(\mathcal{B}',max,+)$	37.90 ± 0.39	30.68 ± 0.37	24.95 ± 0.41	19.84 ± 0.42	16.27 ± 0.41

intra-block, so in this situation a conservative scheme is more proper. But it gradually changes as payload becomes large.

Our reorganized partition $\mathcal{D}^*$ is also valid for steganographic embedding on JPEG images. Although it does not overwhelm $\mathcal{D}$ as is in detection by MaxSRMd2, it works well in JPEG steganography especially when detected by SCA-GFR.

4.4. Experimental results of using LASSO linear classifier as detector

In previous two subsections we use ensemble classifier as detector, there are other choices for detectors, such as LASSO based linear classifier proposed by Cogranne et al. [38]. We tested proposed and original UNIWARD schemes by this classifier on BOSS V1.02. The experimental results of low-complexity linear classifier are similar to ensemble classifier for SRM, MaxSRMd2 and GFR, but it is slightly better for and SCA-GFR, so we present the experimental results of SCA-GFR in Table 9. The schemes calculated by wavelet db8 and db7 on 0.1–0.3 bpp(bpac) are used in this experiments, and parameters are set by searching via cross validation (see Table 10).

Then tendency of experimental results using low-complexity linear classifier is similar to ensemble classifier. For QF75, proposed schemes 2,4,6 outperform original J-UNIWARD with more superiority than ensemble classifier in this experiment.

4.5. Experiments on ALASKA2

ALASKA2 is the latest image base developed for data hiding community. It has 80000 images, which makes it proper for deep model based steganalysis. We select SRNet [39] and EfficientNet-B0 [40] to evaluate distortion schemes on ALASKA2 of size 256 × 256. We randomly split cover and stego sets to 3 sets respectively containing 56000, 16000, and 4000 cover/stego image pairs for training, testing and validation. In this part we tested UNIWARD with db8 and db7 wavelet in 0.1–0.3 bpp(bpac) payload.

Based on the comparison results of previous two part, we select some of our proposed schemes for experiments of SRNet. For JPEG image, we compare proposed schemes with original J-UNIWARD and J-MIPOD [41]. As we know, J-UNIWARD and J-MIPOD are state-of-the-art distortion schemes for JPEG image and are designed with different principals, we also take into account their fusion via method [22] proposed by Zhou et al. in comparison. Experimental results are presented in Tables 11 and 12. Revised scheme 1 is better than original UNIWARD, perhaps deep-network can better capture the artifacts left by incomplete directions of wavelets. While J-MIPOD is close to J-UNIWARD for gray scale images and its basis is very different to J-UNIWARD, the fusion of J-MIPOD with original and revised J-UNIWARD could gain better results.

For EfficientNet-B0, we tested schemes 1,3,5 for JPEG images, we compared them to original UNIWARD. The experimental results on spatial image is similar to SRNet, so we present results on JPEG images in Table 13. Moreover, we find that if we remove D4 augmentation in training efficient net for original J-UNIWARD, the detection results may promote about 1%–%2 for some cases(denoted as original J-UNIWARD*). Perhaps deep network sometimes can explicitly capture the artifacts better without flipping transform.

4.6. Remarks

In this paper we proposed several merging schemes, and a comprehensive comparison is presented. It seems that the for these schemes,

Table 3
Experimental results P_E on BOSSc_J85 and BOSSc V1.01 detected by SRM.

Wavelet	Method	BOSSc_J85			BOSSc		
		Payload rate			Payload rate		
		0.1	0.2	0.3	0.1	0.2	0.3
db8	Original UNIWARD	27.92 ± 0.32	12.91 ± 0.21	6.42 ± 0.13	31.10 ± 0.31	16.54 ± 0.40	9.39 ± 0.23
	Scheme 1. $(\mathcal{B},+,+)$	28.14 ± 0.38	12.96 ± 0.29	6.66 ± 0.22	31.77 ± 0.34	16.66 ± 0.33	9.69 ± 0.16
	Scheme 2. $(\mathcal{B},max,+)$	28.13 ± 0.26	12.79 ± 0.31	6.79 ± 0.23	31.44 ± 0.42	16.45 ± 0.23	9.55 ± 0.24
	Scheme 3. $(\mathcal{B},min,+)$	28.32 ± 0.31	13.01 ± 0.20	6.60 ± 0.24	31.61 ± 0.40	16.63 ± 0.29	9.63 ± 0.28
	Scheme 4. $(\mathcal{D},+,max)$	28.35 ± 0.52	13.06 ± 0.42	6.51 ± 0.20	31.31 ± 0.39	16.52 ± 0.33	9.55 ± 0.29
	Scheme 5. $(\mathcal{D},+,min)$	28.36 ± 0.49	13.21 ± 0.37	6.69 ± 0.22	*31.89 ± 0.28	16.65 ± 0.28	9.57 ± 0.31
	Scheme 6. $(\mathcal{D}^*,+,max)$	28.35 ± 0.48	13.17 ± 0.32	6.51 ± 0.19	31.70 ± 0.43	16.54 ± 0.31	9.71 ± 0.34
	Scheme 7. $(\mathcal{D}^*,+,min)$	28.46 ± 0.32	13.11 ± 0.27	6.64 ± 0.40	31.71 ± 0.21	16.37 ± 0.25	9.55 ± 0.27
	Scheme 8. $(\mathcal{B}',max,+)$	28.67 ± 0.49	12.84 ± 0.44	6.75 ± 0.27	31.67 ± 0.39	16.63 ± 0.33	**9.72 ± 0.21**
	Original WOW	27.90 ± 0.35	13.28 ± 0.20	6.91 ± 0.24	29.99 ± 0.55	16.34 ± 0.55	9.58 ± 0.38
	Revised WOW	28.21 ± 0.24	13.57 ± 0.30	7.13 ± 0.31	30.07 ± 0.37	16.12 ± 0.29	9.27 ± 0.36
db7	Original UNIWARD	28.35 ± 0.33	13.05 ± 0.39	6.63 ± 0.29	31.26 ± 0.32	16.38 ± 0.30	9.09 ± 0.27
	Scheme 1. $(\mathcal{B},+,+)$	28.65 ± 0.40	13.16 ± 0.26	6.64 ± 0.18	31.71 ± 0.38	16.73 ± 0.38	9.22 ± 0.19
	Scheme 2. $(\mathcal{B},max,+)$	28.56 ± 0.52	13.08 ± 0.19	6.69 ± 0.31	31.52 ± 0.49	16.45 ± 0.35	9.33 ± 0.30
	Scheme 3. $(\mathcal{B},min,+)$	28.78 ± 0.29	13.26 ± 0.26	6.69 ± 0.30	31.67 ± 0.30	16.69 ± 0.41	9.30 ± 0.31
	Scheme 4. $(\mathcal{D},+,max)$	28.40 ± 0.36	13.18 ± 0.36	6.75 ± 0.28	31.57 ± 0.34	16.58 ± 0.50	9.23 ± 0.34
	Scheme 5. $(\mathcal{D},+,min)$	28.77 ± 0.30	12.97 ± 0.32	6.71 ± 0.28	31.12 ± 0.44	16.64 ± 0.34	9.35 ± 0.31
	Scheme 6. $(\mathcal{D}^*,+,max)$	28.61 ± 0.35	13.11 ± 0.54	6.66 ± 0.24	31.47 ± 0.48	16.37 ± 0.26	9.31 ± 0.21
	Scheme 7. $(\mathcal{D}^*,+,min)$	28.98 ± 0.31	13.33 ± 0.41	6.51 ± 0.13	31.64 ± 0.29	16.68 ± 0.29	9.36 ± 0.24
	Scheme 8. $(\mathcal{B}',max,+)$	***29.04 ± 0.32**	13.35 ± 0.29	6.62 ± 0.12	***32.35 ± 0.32**	16.89 ± 0.24	9.28 ± 0.23
	Original WOW	28.17 ± 0.44	13.76 ± 0.33	6.95 ± 0.22	30.55 ± 0.42	16.44 ± 0.45	9.41 ± 0.18
	Revised WOW	28.33 ± 0.56	13.68 ± 0.39	7.27 ± 0.36	30.48 ± 0.38	16.38 ± 0.25	9.55 ± 0.24
db6	Original UNIWARD	28.48 ± 0.31	13.14 ± 0.37	6.74 ± 0.11	31.41 ± 0.32	16.63 ± 0.24	9.20 ± 0.30
	Scheme 1. $(\mathcal{B},+,+)$	28.58 ± 0.32	13.41 ± 0.36	6.88 ± 0.23	31.81 ± 0.45	16.63 ± 0.15	9.50 ± 0.35
	Scheme 2. $(\mathcal{B},max,+)$	28.16 ± 0.24	13.13 ± 0.18	6.86 ± 0.24	31.57 ± 0.37	16.66 ± 0.30	9.50 ± 0.38
	Scheme 3. $(\mathcal{B},min,+)$	28.67 ± 0.38	13.49 ± 0.34	7.03 ± 0.23	31.82 ± 0.44	16.85 ± 0.35	9.66 ± 0.14
	Scheme 4. $(\mathcal{D},+,max)$	28.39 ± 0.36	13.27 ± 0.33	6.66 ± 0.25	31.47 ± 0.41	16.51 ± 0.26	9.26 ± 0.31
	Scheme 5. $(\mathcal{D},+,min)$	28.62 ± 0.31	13.31 ± 0.50	6.90 ± 0.28	31.72 ± 0.56	16.66 ± 0.27	9.26 ± 0.28
	Scheme 6. $(\mathcal{D}^*,+,max)$	28.34 ± 0.33	13.16 ± 0.23	6.89 ± 0.30	31.50 ± 0.46	16.40 ± 0.32	9.22 ± 0.28
	Scheme 7. $(\mathcal{D}^*,+,min)$	28.93 ± 0.39	13.35 ± 0.21	6.84 ± 0.12	32.01 ± 0.33	16.84 ± 0.20	9.51 ± 0.25
	Scheme 8. $(\mathcal{B}',max,+)$	28.72 ± 0.48	13.34 ± 0.23	6.94 ± 0.14	*32.32 ± 0.30	16.89 ± 0.35	9.39 ± 0.36
	Original WOW	27.88 ± 0.42	13.36 ± 0.35	7.30 ± 0.28	30.16 ± 0.25	16.18 ± 0.31	9.34 ± 0.31
	Revised WOW	28.05 ± 0.74	13.45 ± 0.32	7.36 ± 0.17	30.49 ± 0.42	16.28 ± 0.48	9.28 ± 0.25
db5	Original UNIWARD	28.19 ± 0.44	13.16 ± 0.25	6.73 ± 0.23	30.92 ± 0.34	16.48 ± 0.33	9.25 ± 0.28
	Scheme 1. $(\mathcal{B},+,+)$	28.51 ± 0.35	13.59 ± 0.18	6.92 ± 0.21	31.50 ± 0.23	16.63 ± 0.30	9.65 ± 0.31
	Scheme 2. $(\mathcal{B},max,+)$	28.48 ± 0.41	13.39 ± 0.21	6.88 ± 0.21	31.23 ± 0.41	16.48 ± 0.27	9.51 ± 0.31
	Scheme 3. $(\mathcal{B},min,+)$	28.61 ± 0.25	**13.66 ± 0.24**	7.00 ± 0.10	*31.82 ± 0.31	16.80 ± 0.25	9.63 ± 0.29
	Scheme 4. $(\mathcal{D},+,max)$	28.64 ± 0.28	13.40 ± 0.43	6.89 ± 0.20	31.26 ± 0.25	16.42 ± 0.32	9.49 ± 0.31
	Scheme 5. $(\mathcal{D},+,min)$	28.80 ± 0.41	13.47 ± 0.23	6.81 ± 0.21	*31.85 ± 0.29	16.78 ± 0.13	9.62 ± 0.38
	Scheme 6. $(\mathcal{D}^*,+,max)$	28.49 ± 0.51	13.19 ± 0.39	6.84 ± 0.27	31.02 ± 0.30	16.51 ± 0.27	9.53 ± 0.29
	Scheme 7. $(\mathcal{D}^*,+,min)$	28.54 ± 0.28	13.24 ± 0.32	7.00 ± 0.25	31.47 ± 0.48	16.50 ± 0.35	9.70 ± 0.25
	Scheme 8. $(\mathcal{B}',max,+)$	28.59 ± 0.39	13.50 ± 0.30	**7.08 ± 0.20**	31.30 ± 0.38	16.59 ± 0.21	9.50 ± 0.31
	Original WOW	27.41 ± 0.26	13.49 ± 0.31	7.21 ± 0.22	29.30 ± 0.41	15.74 ± 0.34	9.25 ± 0.23
	Revised WOW	27.50 ± 0.31	13.51 ± 0.39	7.14 ± 0.22	28.91 ± 0.48	15.86 ± 0.31	9.11 ± 0.16

the best one varies respect to different settings. However, some schemes consistently exhibit comparable performance to best ones. In our experiment, we tested schemes by feature based and deep-model based steganalysis methods on different datasets. Overall according to experimental results, we suggest some choice presented in Table 14 for steganography on different payload rate and image format.

5. Discussions

In this paper we only consider the isotropically constructed submodels in directions. Although there are possibly more alternative definitions about it in terms of different attributes, such as scale or phase for Gabor filters, they do not have a obvious intrinsic symmetric property. Probably there are some proper merging methods for them, but expensive computational cost is needed for this investigation. Although we still believe the worth of studying them, due to the space of this paper, we leave them to future works.

another question arises as is aforementioned in Section 1, that just by substituting db wavelet filters with other symmetric ones, can we obtain the same or even better results and avoid designing merging methods? This question is particularly meaningful for J-UNIWARD. To answer it, several symmetrization methods have been tried on db wavelet and sym wavelet. The first trial is deliberately symmetrizing db4-db8 wavelet filters by 3 symmetrization methods including adding, subtracting and concatenating filters with their flippings. Unfortunately their performances are very poor perhaps due to deformed spectral after symmetrization. Hence we tried another way by convolving them with their flippings:

$$\widehat{\mathbf{L}} = \mathbf{L} \otimes \mathbf{L}', \quad \widehat{\mathbf{H}} = \mathbf{H} \otimes \mathbf{H}' \tag{22}$$

It can be proved that this operation result in symmetric filters, and in this way the spectral of $\widehat{\mathbf{L}}$ and $\widehat{\mathbf{H}}$ somehow assemble to that of $\mathbf{L}$ and $\mathbf{H}$. However the performance of them has about 3% gap to original UNIWARD in 0.1–0.3 payload rate.

In addition to db wavelet, sym wavelet is a kind of inherent symmetric wavelet which can be used in UNIWARD as a substitution of db wavelet. We tested sym4-sym8, and the performances of them are similar to symmetrization result of db wavelet via Eq. (22), but still no better than db wavelet. Besides, if we apply Eq. (22) to sym wavelet, it is noteworthy that its result would be the same as db wavelet. Perhaps this could somehow strengthen the results of our observations.

Table 4
Experimental results P_E on BOSSc_J85 and BOSSc V1.01 detected by MaxSRMd2.

Wavelet	Method	BOSSc_J85			BOSSc		
		Payload rate			Payload rate		
		0.1	0.2	0.3	0.1	0.2	0.3
db8	Original UNIWARD	27.49 ± 0.27	13.59 ± 0.27	7.50 ± 0.31	29.04 ± 0.35	16.46 ± 0.31	7.94 ± 0.22
	Scheme 1. $(B,+,+)$	27.70 ± 0.23	14.06 ± 0.20	7.63 ± 0.14	29.56 ± 0.31	16.88 ± 0.27	8.13 ± 0.20
	Scheme 2. $(B,max,+)$	*28.56 ± 0.31	13.96 ± 0.16	7.54 ± 0.17	*30.22 ± 0.32	16.92 ± 0.35	8.22 ± 0.18
	Scheme 3. $(B,min,+)$	27.37 ± 0.40	13.70 ± 0.29	7.41 ± 0.21	29.18 ± 0.35	16.23 ± 0.32	8.02 ± 0.20
	Scheme 4. $(D,+,max)$	28.11 ± 0.43	*14.30 ± 0.29	7.59 ± 0.31	***30.25 ± 0.28**	***16.94 ± 0.37**	8.17 ± 0.28
	Scheme 5. $(D,+,min)$	27.44 ± 0.35	13.70 ± 0.28	7.44 ± 0.27	29.00 ± 0.36	16.46 ± 0.21	8.05 ± 0.29
	Scheme 6. $(D^*,+,max)$	28.16 ± 0.43	14.06 ± 0.22	7.56 ± 0.24	29.75 ± 0.25	16.87 ± 0.40	8.27 ± 0.28
	Scheme 7. $(D^*,+,min)$	27.51 ± 0.34	13.82 ± 0.20	7.45 ± 0.31	29.09 ± 0.26	16.39 ± 0.25	8.08 ± 0.29
	Scheme 8. $(B',max,+)$	27.43 ± 0.52	13.47 ± 0.51	7.39 ± 0.22	29.46 ± 0.25	16.45 ± 0.20	7.83 ± 0.23
	Original WOW	22.66 ± 0.34	11.90 ± 0.26	7.11 ± 0.41	22.74 ± 0.48	12.31 ± 0.23	7.34 ± 0.24
	Revised WOW	23.50 ± 0.33	12.18 ± 0.25	7.19 ± 0.34	23.36 ± 0.37	12.51 ± 0.25	7.55 ± 0.34
db7	Original UNIWARD	27.44 ± 0.24	14.01 ± 0.41	7.37 ± 0.25	29.22 ± 0.32	15.41 ± 0.33	8.72 ± 0.27
	Scheme 1. $(B,+,+)$	*28.27 ± 0.35	14.08 ± 0.22	7.62 ± 0.25	29.60 ± 0.30	15.56 ± 0.22	9.05 ± 0.33
	Scheme 2. $(B,max,+)$	*28.62 ± 0.33	14.35 ± 0.37	7.59 ± 0.18	*29.98 ± 0.28	15.90 ± 0.22	8.86 ± 0.22
	Scheme 3. $(B,min,+)$	27.77 ± 0.51	13.95 ± 0.38	7.51 ± 0.33	29.18 ± 0.24	15.38 ± 0.27	8.57 ± 0.25
	Scheme 4. $(D,+,max)$	***28.66 ± 0.37**	14.07 ± 0.32	7.56 ± 0.28	29.82 ± 0.29	15.72 ± 0.33	8.96 ± 0.38
	Scheme 5. $(D,+,min)$	28.05 ± 0.36	14.00 ± 0.38	7.68 ± 0.45	29.45 ± 0.46	15.56 ± 0.38	8.83 ± 0.37
	Scheme 6. $(D^*,+,max)$	*28.17 ± 0.31	14.06 ± 0.22	7.62 ± 0.20	*30.02 ± 0.26	15.87 ± 0.38	8.99 ± 0.25
	Scheme 7. $(D^*,+,min)$	27.91 ± 0.34	13.96 ± 0.33	7.73 ± 0.28	29.16 ± 0.26	15.53 ± 0.23	8.54 ± 0.27
	Scheme 8. $(B',max,+)$	27.94 ± 0.38	13.89 ± 0.37	7.28 ± 0.22	29.39 ± 0.42	15.41 ± 0.23	8.51 ± 0.19
	Original WOW	23.11 ± 0.24	12.33 ± 0.31	7.09 ± 0.30	22.76 ± 0.57	12.22 ± 0.35	7.33 ± 0.28
	Revised WOW	23.53 ± 0.23	12.33 ± 0.33	7.16 ± 0.23	23.00 ± 0.31	12.66 ± 0.30	7.67 ± 0.29
db6	Original UNIWARD	27.83 ± 0.34	14.03 ± 0.22	7.48 ± 0.22	28.69 ± 0.24	15.48 ± 0.34	8.66 ± 0.29
	Scheme 1. $(B,+,+)$	28.43 ± 0.37	14.48 ± 0.27	7.74 ± 0.26	*29.45 ± 0.25	15.72 ± 0.20	9.10 ± 0.39
	Scheme 2. $(B,max,+)$	28.36 ± 0.31	14.24 ± 0.23	7.77 ± 0.31	*29.62 ± 0.43	15.98 ± 0.37	8.85 ± 0.16
	Scheme 3. $(B,min,+)$	27.58 ± 0.35	13.86 ± 0.29	7.63 ± 0.20	28.88 ± 0.41	15.49 ± 0.32	8.55 ± 0.24
	Scheme 4. $(D,+,max)$	28.47 ± 0.38	14.17 ± 0.35	7.70 ± 0.21	*29.68 ± 0.33	15.61 ± 0.22	9.06 ± 0.23
	Scheme 5. $(D,+,min)$	27.90 ± 0.27	14.20 ± 0.14	7.55 ± 0.21	29.26 ± 0.36	15.36 ± 0.30	8.48 ± 0.18
	Scheme 6. $(D^*,+,max)$	28.44 ± 0.35	***14.54 ± 0.25**	7.70 ± 0.19	*29.75 ± 0.31	16.02 ± 0.40	8.95 ± 0.18
	Scheme 7. $(D^*,+,min)$	27.92 ± 0.44	14.06 ± 0.35	7.61 ± 0.27	29.06 ± 0.43	15.74 ± 0.33	8.65 ± 0.22
	Scheme 8. $(B',max,+)$	28.02 ± 0.46	13.90 ± 0.27	7.72 ± 0.33	*29.55 ± 0.29	15.26 ± 0.35	8.44 ± 0.28
	Original WOW	22.91 ± 0.31	12.15 ± 0.26	6.87 ± 0.17	22.65 ± 0.31	12.08 ± 0.21	7.49 ± 0.33
	Revised WOW	23.15 ± 0.37	12.49 ± 0.28	7.19 ± 0.18	22.58 ± 0.44	12.13 ± 0.28	7.35 ± 0.30
db5	Original UNIWARD	27.81 ± 0.40	13.82 ± 0.19	7.63 ± 0.18	28.25 ± 0.34	15.16 ± 0.22	8.62 ± 0.32
	Scheme 1. $(B,+,+)$	27.93 ± 0.24	*14.52 ± 0.34	***7.88 ± 0.39**	*29.13 ± 0.28	15.71 ± 0.31	9.07 ± 0.29
	Scheme 2. $(B,max,+)$	*28.61 ± 0.31	14.33 ± 0.29	7.79 ± 0.35	*29.33 ± 0.30	*15.90 ± 0.31	8.93 ± 0.32
	Scheme 3. $(B,min,+)$	27.36 ± 0.37	14.01 ± 0.35	7.63 ± 0.24	28.33 ± 0.52	15.25 ± 0.26	8.59 ± 0.35
	Scheme 4. $(D,+,max)$	28.31 ± 0.30	14.24 ± 0.31	7.81 ± 0.23	*29.21 ± 0.36	15.88 ± 0.34	8.95 ± 0.22
	Scheme 5. $(D,+,min)$	27.60 ± 0.46	14.10 ± 0.32	7.76 ± 0.24	28.45 ± 0.33	15.20 ± 0.35	8.55 ± 0.30
	Scheme 6. $(D^*,+,max)$	28.29 ± 0.52	14.44 ± 0.29	7.79 ± 0.36	*29.28 ± 0.32	15.68 ± 0.27	***9.14 ± 0.31**
	Scheme 7. $(D^*,+,min)$	27.80 ± 0.31	14.09 ± 0.35	7.73 ± 0.29	28.48 ± 0.57	15.03 ± 0.29	8.64 ± 0.29
	Scheme 8. $(B',max,+)$	27.52 ± 0.34	13.85 ± 0.30	7.62 ± 0.25	28.88 ± 0.26	14.96 ± 0.35	8.97 ± 0.27
	Original WOW	22.43 ± 0.38	11.76 ± 0.21	7.00 ± 0.26	21.64 ± 0.29	11.64 ± 0.30	7.19 ± 0.14
	Revised WOW	22.52 ± 0.22	12.23 ± 0.39	6.86 ± 0.25	21.85 ± 0.34	11.85 ± 0.23	7.34 ± 0.12

Although it is not proper to assert that symmetric filters are helpless since our trials are impossible to cast all of them. However it is heuristically recognized that filter bank with orientation properties generally are more capable to capture image content information and increase the diversity of distortion function, which is important for promoting the performance. This is why we strive to find better merging method for them.

Merging is an important phase in this work. we noticed that CPP rule proposed in [21] remarkably boost the performance by fusing different distortion function schemes for spatial image. So we tried to adopt CPP rule as a option in merging sub-models of proposed scheme. We tested CPP and its combinations with strategies described in Section 3.2, but find the performance degrade. This is understandable because CPP rule is designed for fusing costs from distortion function of heterogeneous mechanism. For homogeneous costs, such "controversy" implies the existence of the "weakness" in certain directions, which makes encouragement of modifying it irrational. However, proposed merging methods can coexist with CPP rule for different levels of combining. With some tentative experiments, we find that for some schemes of revised S-UNIWARD, combination of db5 and db8 can give a promotion of approximately 0.6%–0.8% for each payload rate. This can be ascribed to the fact that db5 and db8 makes the diversity by different scales of reception field.

As described in Section 4.2, the purpose of experiment on BOSSc_J85 is simulating spatial image decompressed from JPEG image generated by built-in compressor of camera, since different camera types may use different quantization table, we also tested S-UNIWARD and its revised schemes on BOSSc_J75 and BOSSc_J95, and received similar results that they outperform WOW especially for detection of MaxSRMd2. Besides, we also tested our schemes on BOSS_J85, in this image base WOW is usually better, and some schemes of revised S-UNIWARD are close to it in detection with MaxSRMd2.

Our schemes inevitably increase computational time for more sub-models. This is severe for J-UNIWARD, so we tested their time cost. In this test, we optimized some procedures of block reading operations based on open source code of J-UNIWARD. For image of 512×512 and 2048×2048, revised J-UNIWARD cost 0.98 s and 15.4 s, while original J-UNIWARD cost 0.35 s and 6.54 s, We also observed the memory allocation cost more time for image of larger size.

In addition to UNIWARD, GUED also use Gabor filters with different directions. This implies that our proposed merging schemes may be applied to GUED. However, directional properties of Gabor filters used

Table 5
Experimental results P_E of J-UNIWARD detected by GFR, Qf = 95.

Wavelet	Method	Payload rate				
		0.1	0.2	0.3	0.4	0.5
db8	Original UNIWARD	47.69 ± 0.17	43.15 ± 0.25	37.13 ± 0.14	30.14 ± 0.37	22.52 ± 0.36
	Scheme 1. $(\mathcal{B},+,+)$	47.77 ± 0.15	43.40 ± 0.16	37.35 ± 0.47	30.22 ± 0.48	22.59 ± 0.23
	Scheme 2. $(\mathcal{B},max,+)$	47.65 ± 0.28	43.15 ± 0.18	36.60 ± 0.45	29.54 ± 0.46	21.52 ± 0.24
	Scheme 3. $(\mathcal{B},min,+)$	47.88 ± 0.17	**43.53 ± 0.26**	37.44 ± 0.13	30.50 ± 0.32	**23.06 ± 0.33**
	Scheme 4. $(D,+,max)$	47.85 ± 0.18	42.98 ± 0.21	36.76 ± 0.16	29.45 ± 0.38	22.01 ± 0.45
	Scheme 5. $(D,+,min)$	47.95 ± 0.22	43.50 ± 0.35	**37.61 ± 0.29**	30.49 ± 0.34	22.96 ± 0.33
	Scheme 6. $(D^*,+,max)$	47.95 ± 0.15	42.98 ± 0.25	36.56 ± 0.16	29.49 ± 0.29	21.75 ± 0.39
	Scheme 7. $(D^*,+,min)$	47.89 ± 0.23	43.30 ± 0.19	37.47 ± 0.20	**30.69 ± 0.31**	22.62 ± 0.33
db7	Original UNIWARD	47.74 ± 0.17	42.97 ± 0.25	36.71 ± 0.36	29.01 ± 0.22	21.59 ± 0.40
	Scheme 1. $(\mathcal{B},+,+)$	47.84 ± 0.19	42.98 ± 0.23	36.78 ± 0.40	29.24 ± 0.22	21.67 ± 0.27
	Scheme 2. $(\mathcal{B},max,+)$	47.68 ± 0.18	42.71 ± 0.22	36.08 ± 0.36	28.43 ± 0.17	20.66 ± 0.28
	Scheme 3. $(\mathcal{B},min,+)$	47.87 ± 0.16	43.22 ± 0.30	37.12 ± 0.16	*29.81 ± 0.24	22.27 ± 0.26
	Scheme 4. $(D,+,max)$	47.62 ± 0.22	42.80 ± 0.35	36.06 ± 0.32	28.66 ± 0.42	20.74 ± 0.43
	Scheme 5. $(D,+,min)$	47.88 ± 0.16	43.31 ± 0.18	37.02 ± 0.30	*29.88 ± 0.37	22.28 ± 0.23
	Scheme 6. $(D^*,+,max)$	47.80 ± 0.20	42.94 ± 0.29	36.28 ± 0.24	28.48 ± 0.38	20.89 ± 0.43
	Scheme 7. $(D^*,+,min)$	47.78 ± 0.17	43.19 ± 0.30	37.04 ± 0.39	29.48 ± 0.34	22.01 ± 0.29
db6	Original UNIWARD	47.87 ± 0.27	43.13 ± 0.37	36.85 ± 0.24	29.34 ± 0.29	21.87 ± 0.41
	Scheme 1. $(\mathcal{B},+,+)$	47.85 ± 0.16	43.20 ± 0.41	36.91 ± 0.32	29.35 ± 0.28	21.89 ± 0.24
	Scheme 2. $(\mathcal{B},max,+)$	47.73 ± 0.19	42.74 ± 0.24	36.13 ± 0.41	28.50 ± 0.27	20.63 ± 0.34
	Scheme 3. $(\mathcal{B},min,+)$	**47.97 ± 0.18**	43.44 ± 0.20	37.30 ± 0.28	*30.31 ± 0.44	*22.60 ± 0.17
	Scheme 4. $(D,+,max)$	47.63 ± 0.12	42.76 ± 0.25	36.26 ± 0.41	28.76 ± 0.25	21.02 ± 0.22
	Scheme 5. $(D,+,min)$	47.77 ± 0.16	43.49 ± 0.17	37.27 ± 0.38	29.95 ± 0.31	22.39 ± 0.28
	Scheme 6. $(D^*,+,max)$	47.77 ± 0.22	42.90 ± 0.34	36.29 ± 0.30	28.71 ± 0.24	21.01 ± 0.20
	Scheme 7. $(D^*,+,min)$	47.84 ± 0.16	43.36 ± 0.27	37.13 ± 0.37	29.85 ± 0.49	22.20 ± 0.17
db5	Original UNIWARD	47.70 ± 0.14	43.09 ± 0.25	36.67 ± 0.22	29.60 ± 0.43	21.92 ± 0.17
	Scheme 1. $(\mathcal{B},+,+)$	47.76 ± 0.15	43.19 ± 0.25	36.79 ± 0.36	29.60 ± 0.33	21.80 ± 0.27
	Scheme 2. $(\mathcal{B},max,+)$	47.66 ± 0.15	42.73 ± 0.26	36.24 ± 0.48	28.77 ± 0.46	20.91 ± 0.24
	Scheme 3. $(\mathcal{B},min,+)$	47.96 ± 0.25	43.29 ± 0.30	*37.24 ± 0.22	30.41 ± 0.32	*22.83 ± 0.30
	Scheme 4. $(D,+,max)$	47.77 ± 0.22	42.96 ± 0.26	36.41 ± 0.25	29.00 ± 0.23	21.09 ± 0.32
	Scheme 5. $(D,+,min)$	47.76 ± 0.24	43.37 ± 0.30	*37.28 ± 0.21	30.22 ± 0.42	22.34 ± 0.30
	Scheme 6. $(D^*,+,max)$	47.73 ± 0.17	43.01 ± 0.15	36.54 ± 0.28	28.89 ± 0.57	21.33 ± 0.18
	Scheme 7. $(D^*,+,min)$	47.88 ± 0.14	43.43 ± 0.41	*37.20 ± 0.22	30.03 ± 0.27	22.47 ± 0.36

Table 6
Experimental results P_E of J-UNIWARD detected by SCA-GFR Qf = 95.

Wavelet	Method	Payload rate				
		0.1	0.2	0.3	0.4	0.5
db8	Original UNIWARD	46.07 ± 0.22	40.23 ± 0.41	33.17 ± 0.30	26.32 ± 0.27	20.02 ± 0.31
	Scheme 1. $(\mathcal{B},+,+)$	46.31 ± 0.27	40.30 ± 0.25	33.47 ± 0.30	26.52 ± 0.18	20.37 ± 0.27
	Scheme 2. $(\mathcal{B},max,+)$	46.17 ± 0.17	40.01 ± 0.37	33.09 ± 0.23	26.00 ± 0.18	19.27 ± 0.19
	Scheme 3. $(\mathcal{B},min,+)$	46.40 ± 0.22	40.38 ± 0.26	33.63 ± 0.28	***27.21 ± 0.26**	***20.69 ± 0.24**
	Scheme 4. $(D,+,max)$	46.05 ± 0.34	40.15 ± 0.36	33.17 ± 0.27	25.66 ± 0.31	19.48 ± 0.20
	Scheme 5. $(D,+,min)$	46.28 ± 0.41	40.50 ± 0.35	33.52 ± 0.23	26.79 ± 0.28	20.47 ± 0.40
	Scheme 6. $(D^*,+,max)$	46.24 ± 0.33	40.15 ± 0.26	32.99 ± 0.45	26.05 ± 0.25	19.45 ± 0.36
	Scheme 7. $(D^*,+,min)$	46.16 ± 0.25	40.40 ± 0.18	33.66 ± 0.29	26.62 ± 0.44	20.63 ± 0.26
db7	Original UNIWARD	46.05 ± 0.31	40.10 ± 0.37	33.06 ± 0.27	25.71 ± 0.27	19.15 ± 0.25
	Scheme 1. $(\mathcal{B},+,+)$	46.53 ± 0.31	40.41 ± 0.31	33.11 ± 0.39	25.77 ± 0.39	19.38 ± 0.27
	Scheme 2. $(\mathcal{B},max,+)$	46.43 ± 0.26	40.09 ± 0.32	32.64 ± 0.33	25.35 ± 0.24	18.35 ± 0.30
	Scheme 3. $(\mathcal{B},min,+)$	46.30 ± 0.26	40.26 ± 0.26	33.28 ± 0.26	*26.41 ± 0.30	*20.11 ± 0.29
	Scheme 4. $(D,+,max)$	46.56 ± 0.24	40.19 ± 0.31	32.86 ± 0.31	25.33 ± 0.24	18.44 ± 0.28
	Scheme 5. $(D,+,min)$	46.26 ± 0.25	40.25 ± 0.30	33.26 ± 0.22	*26.46 ± 0.21	*19.96 ± 0.36
	Scheme 6. $(D^*,+,max)$	46.41 ± 0.20	40.46 ± 0.24	32.58 ± 0.33	25.14 ± 0.36	18.55 ± 0.14
	Scheme 7. $(D^*,+,min)$	46.24 ± 0.28	40.20 ± 0.30	33.40 ± 0.30	*26.44 ± 0.27	*19.95 ± 0.19
db6	Original UNIWARD	46.39 ± 0.19	40.31 ± 0.28	33.22 ± 0.19	26.21 ± 0.21	19.70 ± 0.28
	Scheme 1. $(\mathcal{B},+,+)$	46.36 ± 0.26	40.36 ± 0.36	33.46 ± 0.38	26.27 ± 0.16	19.62 ± 0.20
	Scheme 2. $(\mathcal{B},max,+)$	46.32 ± 0.30	40.39 ± 0.28	32.70 ± 0.36	25.43 ± 0.29	18.76 ± 0.21
	Scheme 3. $(\mathcal{B},min,+)$	46.42 ± 0.29	40.50 ± 0.36	33.50 ± 0.32	26.67 ± 0.37	*20.44 ± 0.30
	Scheme 4. $(D,+,max)$	46.43 ± 0.22	40.43 ± 0.26	33.18 ± 0.42	25.40 ± 0.26	18.77 ± 0.35
	Scheme 5. $(D,+,min)$	46.45 ± 0.20	40.52 ± 0.34	33.69 ± 0.43	26.72 ± 0.37	20.13 ± 0.20
	Scheme 6. $(D^*,+,max)$	46.67 ± 0.28	40.49 ± 0.20	32.80 ± 0.20	25.63 ± 0.25	18.77 ± 0.32
	Scheme 7. $(D^*,+,min)$	46.52 ± 0.11	40.57 ± 0.31	33.52 ± 0.29	26.64 ± 0.43	20.40 ± 0.43
db5	Original UNIWARD	46.25 ± 0.19	40.45 ± 0.30	33.31 ± 0.23	26.64 ± 0.34	20.05 ± 0.25
	Scheme 1. $(\mathcal{B},+,+)$	46.61 ± 0.38	40.61 ± 0.32	33.67 ± 0.36	26.54 ± 0.45	19.94 ± 0.39
	Scheme 2. $(\mathcal{B},max,+)$	46.25 ± 0.34	40.70 ± 0.26	32.93 ± 0.17	25.72 ± 0.33	18.91 ± 0.19
	Scheme 3. $(\mathcal{B},min,+)$	46.57 ± 0.19	40.58 ± 0.32	33.76 ± 0.31	26.93 ± 0.26	20.51 ± 0.31
	Scheme 4. $(D,+,max)$	46.50 ± 0.30	40.32 ± 0.25	33.34 ± 0.46	25.71 ± 0.31	18.90 ± 0.28
	Scheme 5. $(D,+,min)$	**46.70 ± 0.26**	40.66 ± 0.23	*33.90 ± 0.17	26.87 ± 0.47	20.50 ± 0.24
	Scheme 6. $(D^*,+,max)$	46.40 ± 0.20	40.53 ± 0.42	33.24 ± 0.45	25.92 ± 0.43	18.98 ± 0.32
	Scheme 7. $(D^*,+,min)$	46.61 ± 0.28	**40.78 ± 0.36**	***33.98 ± 0.34**	27.08 ± 0.27	20.63 ± 0.31

Table 7
Experimental results P_E of J-UNIWARD detected by GFR, Qf = 75.

Wavelet	Method	Payload rate				
		0.1	0.2	0.3	0.4	0.5
db8	Original UNIWARD	40.77 ± 0.28	28.26 ± 0.33	17.73 ± 0.37	10.07 ± 0.19	5.15 ± 0.16
	Scheme 1. $(\mathcal{B}, +, +)$	40.99 ± 0.44	28.66 ± 0.38	17.98 ± 0.28	10.20 ± 0.38	5.50 ± 0.26
	Scheme 2. $(\mathcal{B}, max, +)$	40.76 ± 0.29	28.24 ± 0.31	17.08 ± 0.36	9.39 ± 0.29	4.89 ± 0.12
	Scheme 3. $(\mathcal{B}, min, +)$	41.14 ± 0.29	28.84 ± 0.22	**18.22 ± 0.31**	*__10.66 ± 0.22__	**5.62 ± 0.17**
	Scheme 4. $(\mathcal{D}, +, max)$	40.76 ± 0.25	28.32 ± 0.42	17.13 ± 0.28	9.74 ± 0.19	5.05 ± 0.13
	Scheme 5. $(\mathcal{D}, +, min)$	41.09 ± 0.29	**28.97 ± 0.33**	18.09 ± 0.21	10.52 ± 0.20	5.58 ± 0.22
	Scheme 6. $(\mathcal{D}^*, +, max)$	40.86 ± 0.31	28.23 ± 0.33	17.31 ± 0.35	9.65 ± 0.22	5.06 ± 0.19
	Scheme 7. $(\mathcal{D}^*, +, min)$	41.02 ± 0.43	28.79 ± 0.21	18.09 ± 0.43	10.58 ± 0.21	5.61 ± 0.20
db7	Original UNIWARD	40.51 ± 0.28	27.71 ± 0.42	16.91 ± 0.24	9.24 ± 0.22	4.90 ± 0.27
	Scheme 1. $(\mathcal{B}, +, +)$	40.56 ± 0.26	27.94 ± 0.35	16.97 ± 0.31	9.43 ± 0.19	4.88 ± 0.24
	Scheme 2. $(\mathcal{B}, max, +)$	40.47 ± 0.25	27.54 ± 0.35	16.40 ± 0.31	8.76 ± 0.17	4.43 ± 0.18
	Scheme 3. $(\mathcal{B}, min, +)$	40.88 ± 0.42	28.20 ± 0.25	17.43 ± 0.25	9.79 ± 0.28	5.13 ± 0.17
	Scheme 4. $(\mathcal{D}, +, max)$	40.46 ± 0.30	27.91 ± 0.28	16.70 ± 0.23	8.85 ± 0.15	4.53 ± 0.25
	Scheme 5. $(\mathcal{D}, +, min)$	40.91 ± 0.45	28.44 ± 0.36	17.45 ± 0.21	9.71 ± 0.29	5.26 ± 0.19
	Scheme 6. $(\mathcal{D}^*, +, max)$	40.64 ± 0.36	27.56 ± 0.31	16.47 ± 0.26	8.96 ± 0.27	4.48 ± 0.12
	Scheme 7. $(\mathcal{D}^*, +, min)$	41.06 ± 0.45	28.04 ± 0.31	17.08 ± 0.42	9.77 ± 0.29	5.06 ± 0.26
db6	Original UNIWARD	40.86 ± 0.26	28.04 ± 0.25	17.09 ± 0.23	9.52 ± 0.20	4.90 ± 0.18
	Scheme 1. $(\mathcal{B}, +, +)$	40.88 ± 0.24	28.44 ± 0.27	17.31 ± 0.33	9.68 ± 0.22	5.06 ± 0.20
	Scheme 2. $(\mathcal{B}, max, +)$	40.61 ± 0.49	27.72 ± 0.38	16.73 ± 0.21	9.13 ± 0.22	4.66 ± 0.09
	Scheme 3. $(\mathcal{B}, min, +)$	41.07 ± 0.27	28.54 ± 0.23	*17.97 ± 0.38	9.96 ± 0.30	5.34 ± 0.16
	Scheme 4. $(\mathcal{D}, +, max)$	40.82 ± 0.38	27.94 ± 0.32	17.14 ± 0.41	9.25 ± 0.15	4.79 ± 0.23
	Scheme 5. $(\mathcal{D}, +, min)$	41.00 ± 0.35	28.40 ± 0.21	17.58 ± 0.27	9.99 ± 0.24	5.31 ± 0.25
	Scheme 6. $(\mathcal{D}^*, +, max)$	40.45 ± 0.36	27.87 ± 0.37	16.93 ± 0.31	9.11 ± 0.29	4.68 ± 0.14
	Scheme 7. $(\mathcal{D}^*, +, min)$	**41.19 ± 0.38**	28.58 ± 0.29	17.60 ± 0.22	*10.01 ± 0.14	5.50 ± 0.28
db5	Original UNIWARD	40.51 ± 0.28	28.08 ± 0.39	17.02 ± 0.19	9.65 ± 0.29	5.03 ± 0.16
	Scheme 1. $(\mathcal{B}, +, +)$	41.11 ± 0.39	28.62 ± 0.30	17.47 ± 0.37	9.74 ± 0.22	5.09 ± 0.18
	Scheme 2. $(\mathcal{B}, max, +)$	40.64 ± 0.38	27.83 ± 0.25	16.74 ± 0.30	9.11 ± 0.29	4.69 ± 0.14
	Scheme 3. $(\mathcal{B}, min, +)$	41.15 ± 0.34	28.64 ± 0.26	17.55 ± 0.32	10.18 ± 0.24	5.36 ± 0.18
	Scheme 4. $(\mathcal{D}, +, max)$	40.96 ± 0.50	27.65 ± 0.28	16.85 ± 0.40	9.29 ± 0.19	4.70 ± 0.21
	Scheme 5. $(\mathcal{D}, +, min)$	41.12 ± 0.30	28.76 ± 0.37	*17.88 ± 0.28	9.95 ± 0.33	5.38 ± 0.06
	Scheme 6. $(\mathcal{D}^*, +, max)$	40.75 ± 0.38	27.93 ± 0.35	17.11 ± 0.29	9.06 ± 0.23	4.77 ± 0.23
	Scheme 7. $(\mathcal{D}^*, +, min)$	41.10 ± 0.31	28.59 ± 0.29	17.60 ± 0.29	10.01 ± 0.23	5.47 ± 0.21

Table 8
Experimental results P_E of J-UNIWARD detected by SCA-GFR, Qf = 75.

Wavelet	Method	Payload rate				
		0.1	0.2	0.3	0.4	0.5
db8	Original UNIWARD	35.93 ± 0.35	23.10 ± 0.21	14.03 ± 0.24	8.22 ± 0.33	4.50 ± 0.23
	Scheme 1. $(\mathcal{B}, +, +)$	36.47 ± 0.32	23.41 ± 0.25	14.31 ± 0.21	8.33 ± 0.19	4.58 ± 0.28
	Scheme 2. $(\mathcal{B}, max, +)$	36.70 ± 0.37	23.60 ± 0.30	14.15 ± 0.32	7.87 ± 0.15	4.29 ± 0.14
	Scheme 3. $(\mathcal{B}, min, +)$	35.85 ± 0.35	23.28 ± 0.23	14.05 ± 0.14	**8.41 ± 0.33**	4.65 ± 0.13
	Scheme 4. $(\mathcal{D}, +, max)$	*36.83 ± 0.24	23.53 ± 0.48	14.12 ± 0.19	8.15 ± 0.25	4.35 ± 0.21
	Scheme 5. $(\mathcal{D}, +, min)$	35.90 ± 0.41	23.26 ± 0.25	14.09 ± 0.16	8.16 ± 0.21	4.67 ± 0.16
	Scheme 6. $(\mathcal{D}^*, +, max)$	*36.66 ± 0.26	*23.75 ± 0.33	14.17 ± 0.13	8.06 ± 0.19	4.58 ± 0.15
	Scheme 7. $(\mathcal{D}^*, +, min)$	36.14 ± 0.34	23.35 ± 0.28	14.16 ± 0.31	8.34 ± 0.19	4.57 ± 0.19
db7	Original UNIWARD	35.76 ± 0.21	22.34 ± 0.43	13.44 ± 0.33	7.90 ± 0.26	4.09 ± 0.13
	Scheme 1. $(\mathcal{B}, +, +)$	36.27 ± 0.31	23.21 ± 0.47	13.98 ± 0.32	8.13 ± 0.17	4.13 ± 0.13
	Scheme 2. $(\mathcal{B}, max, +)$	*36.64 ± 0.24	23.35 ± 0.41	13.47 ± 0.21	7.90 ± 0.16	4.14 ± 0.18
	Scheme 3. $(\mathcal{B}, min, +)$	35.77 ± 0.22	22.82 ± 0.31	13.67 ± 0.32	8.27 ± 0.16	4.27 ± 0.14
	Scheme 4. $(\mathcal{D}, +, max)$	*36.49 ± 0.25	*23.51 ± 0.37	13.55 ± 0.18	8.00 ± 0.21	4.02 ± 0.23
	Scheme 5. $(\mathcal{D}, +, min)$	36.06 ± 0.32	22.78 ± 0.33	13.53 ± 0.30	8.09 ± 0.20	4.32 ± 0.19
	Scheme 6. $(\mathcal{D}^*, +, max)$	*36.71 ± 0.37	23.13 ± 0.33	13.70 ± 0.34	7.98 ± 0.21	4.01 ± 0.09
	Scheme 7. $(\mathcal{D}^*, +, min)$	35.77 ± 0.23	22.85 ± 0.27	13.73 ± 0.20	8.21 ± 0.31	4.37 ± 0.19
db6	Original UNIWARD	35.91 ± 0.36	22.81 ± 0.23	13.82 ± 0.22	7.82 ± 0.15	4.20 ± 0.13
	Scheme 1. $(\mathcal{B}, +, +)$	36.50 ± 0.34	*23.70 ± 0.34	14.26 ± 0.19	8.07 ± 0.15	4.28 ± 0.17
	Scheme 2. $(\mathcal{B}, max, +)$	*36.89 ± 0.21	23.54 ± 0.36	14.07 ± 0.38	7.84 ± 0.19	4.24 ± 0.13
	Scheme 3. $(\mathcal{B}, min, +)$	35.67 ± 0.24	22.81 ± 0.31	13.95 ± 0.28	8.27 ± 0.25	4.35 ± 0.12
	Scheme 4. $(\mathcal{D}, +, max)$	*__37.20 ± 0.37__	23.27 ± 0.30	13.93 ± 0.22	7.83 ± 0.28	4.28 ± 0.24
	Scheme 5. $(\mathcal{D}, +, min)$	36.29 ± 0.44	23.10 ± 0.32	13.97 ± 0.28	7.98 ± 0.21	4.45 ± 0.30
	Scheme 6. $(\mathcal{D}^*, +, max)$	*36.91 ± 0.38	*23.80 ± 0.12	14.02 ± 0.33	7.93 ± 0.18	4.19 ± 0.14
	Scheme 7. $(\mathcal{D}^*, +, min)$	36.19 ± 0.30	22.81 ± 0.17	13.76 ± 0.27	8.13 ± 0.14	4.55 ± 0.16
db5	Original UNIWARD	35.90 ± 0.26	23.17 ± 0.32	13.84 ± 0.31	7.89 ± 0.24	4.43 ± 0.15
	Scheme 1. $(\mathcal{B}, +, +)$	*36.92 ± 0.30	23.60 ± 0.27	**14.48 ± 0.27**	8.13 ± 0.17	4.51 ± 0.14
	Scheme 2. $(\mathcal{B}, max, +)$	*36.74 ± 0.44	23.60 ± 0.35	14.07 ± 0.18	7.90 ± 0.16	4.24 ± 0.12
	Scheme 3. $(\mathcal{B}, min, +)$	36.30 ± 0.39	23.11 ± 0.32	14.12 ± 0.30	8.29 ± 0.16	4.50 ± 0.16
	Scheme 4. $(\mathcal{D}, +, max)$	*36.92 ± 0.26	23.72 ± 0.34	14.18 ± 0.28	8.00 ± 0.21	4.32 ± 0.18
	Scheme 5. $(\mathcal{D}, +, min)$	36.43 ± 0.32	23.42 ± 0.53	14.08 ± 0.34	8.09 ± 0.20	4.53 ± 0.10
	Scheme 6. $(\mathcal{D}^*, +, max)$	*36.83 ± 0.30	**23.85 ± 0.34**	14.09 ± 0.30	7.98 ± 0.21	4.29 ± 0.16
	Scheme 7. $(\mathcal{D}^*, +, min)$	36.20 ± 0.43	23.48 ± 0.40	14.04 ± 0.37	8.21 ± 0.31	**4.67 ± 0.20**

Table 9
Experimental results of SCA-GFR on JPEG using LASSO linear classifier.

Wavelet	Method	QF75			QF95		
		Payload rate			Payload rate		
		0.1	0.2	0.3	0.1	0.2	0.3
db8	Original UNIWARD	35.75 ± 0.0036	22.49 ± 0.0029	13.58 ± 0.0050	46.62 ± 0.0032	39.86 ± 0.0019	33.00 ± 0.0024
	Scheme 1. $(\mathcal{B}, +, +)$	36.39 ± 0.0017	22.76 ± 0.0014	13.51 ± 0.0032	46.58 ± 0.0027	40.17 ± 0.0020	33.06 ± 0.0017
	Scheme 2. $(\mathcal{B}, max, +)$	36.71 ± 0.0026	23.17 ± 0.0033	13.47 ± 0.0050	46.31 ± 0.0022	39.86 ± 0.0031	32.84 ± 0.0033
	Scheme 3. $(\mathcal{B}, min, +)$	35.46 ± 0.0026	22.57 ± 0.0019	13.62 ± 0.0019	46.55 ± 0.0015	39.93 ± 0.0022	33.57 ± 0.0033
	Scheme 4. $(\mathcal{D}, +, max)$	36.50 ± 0.0019	22.98 ± 0.0029	13.46 ± 0.0026	46.42 ± 0.0022	39.95 ± 0.0020	32.90 ± 0.0015
	Scheme 5. $(\mathcal{D}, +, min)$	35.56 ± 0.0017	22.71 ± 0.0020	13.72 ± 0.0013	46.58 ± 0.0019	39.87 ± 0.0016	33.29 ± 0.0017
	Scheme 6. $(\mathcal{D}^*, +, max)$	36.70 ± 0.0032	22.68 ± 0.0039	13.58 ± 0.0016	46.40 ± 0.0026	40.19 ± 0.0038	32.72 ± 0.0031
	Scheme 7. $(\mathcal{D}^*, +, min)$	35.67 ± 0.0012	22.53 ± 0.0029	13.63 ± 0.0021	46.65 ± 0.0021	40.02 ± 0.0021	33.46 ± 0.0017
db7	Original UNIWARD	35.50 ± 0.0030	22.06 ± 0.0031	12.84 ± 0.0021	46.31 ± 0.0023	39.62 ± 0.0025	32.59 ± 0.0026
	Scheme 1. $(\mathcal{B}, +, +)$	36.48 ± 0.0024	22.52 ± 0.0014	13.16 ± 0.0025	46.45 ± 0.0024	40.07 ± 0.0025	32.83 ± 0.0022
	Scheme 2. $(\mathcal{B}, max, +)$	37.02 ± 0.0037	22.70 ± 0.0028	13.07 ± 0.0019	46.62 ± 0.0027	39.85 ± 0.0021	32.32 ± 0.0024
	Scheme 3. $(\mathcal{B}, min, +)$	35.52 ± 0.0020	22.27 ± 0.0023	13.01 ± 0.0029	46.71 ± 0.0019	40.04 ± 0.0032	33.11 ± 0.0023
	Scheme 4. $(\mathcal{D}, +, max)$	36.65 ± 0.0039	22.76 ± 0.0032	13.08 ± 0.0027	46.44 ± 0.0020	39.80 ± 0.0016	32.43 ± 0.0017
	Scheme 5. $(\mathcal{D}, +, min)$	35.74 ± 0.0026	22.20 ± 0.0024	13.15 ± 0.0023	46.61 ± 0.0017	40.07 ± 0.0017	33.05 ± 0.0026
	Scheme 6. $(\mathcal{D}^*, +, max)$	36.87 ± 0.0038	22.69 ± 0.0016	13.01 ± 0.0025	46.37 ± 0.0024	39.90 ± 0.0014	32.58 ± 0.0020
	Scheme 7. $(\mathcal{D}^*, +, min)$	36.00 ± 0.0021	22.38 ± 0.0027	13.25 ± 0.0023	46.40 ± 0.0023	39.92 ± 0.0019	33.19 ± 0.0026

Table 10
Experimental results of GFR on JPEG using LASSO linear classifier.

Wavelet	Method	QF75			QF95		
		Payload rate			Payload rate		
		0.1	0.2	0.3	0.1	0.2	0.3
db8	Original UNIWARD	41.38 ± 0.0017	28.57 ± 0.0036	17.52 ± 0.0039	47.19 ± 0.0011	41.95 ± 0.0022	35.70 ± 0.0055
	Scheme 1. $(\mathcal{B}, +, +)$	41.22 ± 0.0015	29.00 ± 0.0022	17.76 ± 0.0020	47.19 ± 0.0019	42.10 ± 0.0018	35.65 ± 0.0032
	Scheme 2. $(\mathcal{B}, max, +)$	41.14 ± 0.0033	28.59 ± 0.0034	17.00 ± 0.0020	47.10 ± 0.0020	41.77 ± 0.0019	35.03 ± 0.0041
	Scheme 3. $(\mathcal{B}, min, +)$	41.60 ± 0.0043	29.33 ± 0.0030	18.49 ± 0.0042	47.27 ± 0.0017	42.28 ± 0.0024	36.27 ± 0.0018
	Scheme 4. $(\mathcal{D}, +, max)$	41.27 ± 0.0023	28.49 ± 0.0025	17.25 ± 0.0022	47.12 ± 0.0018	41.75 ± 0.0022	34.92 ± 0.0023
	Scheme 5. $(\mathcal{D}, +, min)$	41.39 ± 0.0026	29.25 ± 0.0042	18.31 ± 0.0028	47.28 ± 0.0019	42.32 ± 0.0016	36.16 ± 0.0037
	Scheme 6. $(\mathcal{D}^*, +, max)$	41.21 ± 0.0022	28.28 ± 0.0032	17.39 ± 0.0025	47.17 ± 0.0013	41.69 ± 0.0027	34.86 ± 0.0026
	Scheme 7. $(\mathcal{D}^*, +, min)$	41.40 ± 0.0027	29.12 ± 0.0033	18.33 ± 0.0041	47.19 ± 0.0021	42.17 ± 0.0019	36.12 ± 0.0017
db7	Original UNIWARD	41.03 ± 0.0024	27.94 ± 0.0041	16.57 ± 0.0024	46.99 ± 0.0017	41.59 ± 0.0015	34.86 ± 0.0024
	Scheme 1. $(\mathcal{B}, +, +)$	41.33 ± 0.0029	28.59 ± 0.0035	17.07 ± 0.0041	47.07 ± 0.0021	41.65 ± 0.0023	34.91 ± 0.0030
	Scheme 2. $(\mathcal{B}, max, +)$	40.88 ± 0.0022	27.99 ± 0.0052	16.06 ± 0.0018	47.17 ± 0.0018	41.25 ± 0.0016	34.01 ± 0.0023
	Scheme 3. $(\mathcal{B}, min, +)$	41.47 ± 0.0028	28.84 ± 0.0038	17.38 ± 0.0014	47.19 ± 0.0016	42.13 ± 0.0028	35.52 ± 0.0024
	Scheme 4. $(\mathcal{D}, +, max)$	41.18 ± 0.0024	27.86 ± 0.0039	16.34 ± 0.0026	47.13 ± 0.0022	41.60 ± 0.0045	34.26 ± 0.0031
	Scheme 5. $(\mathcal{D}, +, min)$	41.25 ± 0.0014	28.54 ± 0.0020	17.27 ± 0.0029	47.20 ± 0.0023	41.97 ± 0.0019	35.60 ± 0.0039
	Scheme 6. $(\mathcal{D}^*, +, max)$	41.05 ± 0.0026	28.21 ± 0.0047	16.31 ± 0.0022	46.98 ± 0.0018	41.38 ± 0.0020	34.22 ± 0.0026
	Scheme 7. $(\mathcal{D}^*, +, min)$	41.30 ± 0.0025	28.67 ± 0.0040	17.28 ± 0.0022	47.09 ± 0.0019	42.17 ± 0.0019	35.50 ± 0.0029

Table 11
Experimental results on ALASKA2 for JPEG by SRNet.

Wavelet	Method	qf75			qf95		
		Payload rate			Payload rate		
		0.1	0.2	0.3	0.1	0.2	0.3
db8	Original UNIWARD	33.72	19.42	13.67	44.76	37.98	27.82
	Scheme 1. $(\mathcal{B}, +, +)$	34.20	19.81	13.73	45.20	38.27	28.18
	Scheme 3. $(\mathcal{B}, min, +)$	34.07	19.93	14.17	45.10	38.30	27.87
	Scheme 5. $(\mathcal{D}, +, min)$	33.67	19.83	13.76	44.89	38.49	28.33
	J-MIPOD	33.37	19.24	13.42	44.69	37.86	27.91
	Original UNIWARD + J-MIPOD	33.98	19.82	13.78	44.98	38.35	28.02
	Scheme 1 + J-MIPOD	34.42	19.91	13.82	45.45	38.48	28.14
db7	Original UNIWARD	33.64	19.48	13.72	44.63	37.84	27.87
	Scheme 1. $(\mathcal{B}, +, +)$	33.91	19.82	13.90	44.87	37.97	28.21
	Scheme 3. $(\mathcal{B}, min, +)$	33.79	19.78	13.86	44.90	38.03	27.99
	Scheme 5. $(\mathcal{D}, +, min)$	33.88	19.62	13.95	44.89	38.08	28.01
	J-MIPOD	33.47	19.24	13.42	44.69	37.86	27.91
	Original UNIWARD + J-MIPOD	33.85	19.71	13.93	44.80	38.02	27.99
	Scheme 1 + J-MIPOD	34.01	19.95	13.88	44.96	38.11	28.24

by GUED are different to UNIWARD because they have 32 directions in $i \times \pi/32, i = 0, 1, \ldots, 31$. Probably the merging strategy "min" and "max" can be applied to symmetric direction such as merging $i \times \pi/32$ with $\pi/2 - i \times \pi/32, i = 0, 1, \ldots, 31$, or with $\pi/2 + i \times \pi/32, i = 0, 1, \ldots, 31$. However, how to further merging submodels from asymmetric directions and different scales, needs more investigations.

6. Conclusion

In this paper we revised UNIWARD distortion function and proposed several merging schemes for submodels. Experimental results demonstrate that our schemes can improve UNIWARD distortion, especially in detection by select-channel feature and deep-model. For some merging schemes' promotion is limited partly because they are akin to original

Table 12
Experimental results on ALASKA2 for spatial image by SRNET.

Wavelet	Method	Payload rate		
		0.1	0.2	0.3
db8	Original S-UNI	32.35	22.16	15.63
	Scheme 1. $(\mathcal{B},+,+)$	32.56	22.54	15.76
	Scheme 5. $(\mathcal{D},+,min)$	32.29	22.10	15.68
	Scheme 6. $(\mathcal{D}^*,+,max)$	33.01	22.89	16.23
db7	Original S-UNI	32.50	22.32	15.01
	Scheme 1. $(\mathcal{B},+,+)$	32.61	22.45	15.34
	Scheme 5. $(\mathcal{D},+,min)$	32.48	22.59	15.08
	Scheme 6. $(\mathcal{D}^*,+,max)$	33.05	22.83	15.68

Table 13
Experimental results on ALASKA2 for JPEG by EfficientNet-B0.

Wavelet	Method	qf75			qf95		
		Payload rate			Payload rate		
		0.1	0.2	0.3	0.1	0.2	0.3
db8	Original UNIWARD	37.16	24.57	17.36	48.89	41.54	31.98
	Original UNIWARD*	36.24	23.14	15.38	48.52	40.86	31.31
	Scheme 1. $(\mathcal{B},+,+)$	36.85	24.87	17.91	48.78	42.11	32.56
	Scheme 3. $(\mathcal{B},min,+)$	37.67	25.09	18.12	48.97	42.32	32.55
	Scheme 5. $(\mathcal{D},+,min)$	37.25	24.75	17.83	48.92	41.74	32.65
db7	Original UNIWARD	36.87	24.65	17.27	48.86	40.97	31.39
	Original UNIWARD*	36.11	23.23	15.29	48.31	40.36	30.67
	Scheme 1. $(\mathcal{B},+,+)$	37.05	24.68	17.70	48.94	41.12	31.66
	Scheme 3. $(\mathcal{B},min,+)$	37.21	24.79	17.93	49.10	41.21	31.92
	Scheme 5. $(\mathcal{D},+,min)$	37.14	24.83	17.81	48.94	41.09	31.74

Table 14
Suggestions of merging schemes.

Image format	Payload rate	Scheme
spatial	All	(db8,Scheme6)
spatial*	All	Scheme4, Scheme8
JPEG QF95	≥0.2	(db8,Scheme1)
JPEG QF95	<0.2	(db8,Scheme3)
JPEG QF75	All	Scheme3

UNIWARD in feature for certain conditions. However it can be easily implemented by modifying original UNIWARD without much efforts. And it do not introduce any extra parameters thus evades any worry about tuning parameters for different kinds of cover images. As we know, in many steganographic techniques UNIWARD is used as a indispensable part. Consequently these methods are also expected to work well on revised UNIWARD. So far, less work focus on merging methods particularly for homogeneous sub-models, we believe this is important because using residuals with orientation in distortion function is common and keep it unbiased for directions is reasonable for avoiding possible defects. From experiments, we can see the merging strategy is important for performance enhancement, and they show their different behaviors for different image data and different steganalysis detection methods, which is important for countering the oracle attacking. This inspires us consider more effective merging methods. There are several issues worth further studying: (1) In this paper, our hierarchical merging method is build on partition of expanded wavelet set $\mathcal{W}'$, but try to allow some overlapping among subsets is also a feasible approach for more complex distortion schemes such as Gabor filter bank based distortions. (2) Integrating merging methods into deep model based distortion generation method to gain better performance.

Declaration of competing interest

The authors declare that they have no known competing financial interests or personal relationships that could have appeared to influence the work reported in this paper.

Acknowledgments

This work was supported in part by the Natural Science Foundation of China under Grant U1936114, 62002334, 62072421 and 62002003; Natural Science Foundation of Fujian Province, China: 2020J01698 and 2017J01761.The Education and Scientific Research Project for Young Middle-aged Teachers in Fujian Province, China: JAT190314. We also thank Guorui Feng and Shunquan Tan for helpful discussions.

References

[1] T. Filler, J. Judas, J. Fridrich, Minimizing additive distortion in steganography using syndrome-trellis codes, IEEE Trans. Inf. Forensics Secur. 6 (3) (2011) 920–935.
[2] G. Feng, X. Zhang, Y. Ren, Z. Qian, S. Li, Diversity-based cascade filters for JPEG steganalysis, IEEE Trans. Circuits Syst. Video Technol. (2019) 1–11, http://dx.doi.org/10.1109/TCSVT.2019.2891778.
[3] X. Song, F. Liu, C. Yang, X. Luo, Y. Zhang, Steganalysis of adaptive JPEG steganography using 2D gabor filters, in: Proc. 3rd ACM Workshop Inf. Hiding Multimedia Security, Portland, OR, USA, 2015, pp. 15–23.
[4] J. Kodovský, J. Fridrich, Steganalysis of JPEG images using rich models, in: Proc. SPIE, 8303, Burlingame, CA, USA, 2012, pp. 83030A–1–83030A–13.
[5] T. Denemark, V. Sedighi, V. Holub, R. Cogranne, J. Fridrich, Selection-channel-aware rich model for steganalysis of digital images, in: 2014 IEEE International Workshop on Information Forensics and Security (WIFS), 2014, pp. 48–53, http://dx.doi.org/10.1109/WIFS.2014.7084302.
[6] J. Zeng, S. Tan, B. Li, J. Huang, Large-scale JPEG image steganalysis using hybrid deep-learning framework, IEEE Trans. Inf. Forensics Secur. 13 (5) (2018) 1200–1214.
[7] T.D. Denemark, M. Boroumand, J. Fridrich, Steganalysis features for content-adaptive JPEG steganography, IEEE Trans. Inf. Forensics Secur. 11 (8) (2016) 1736–1746.
[8] J. Fridrich, J. Kodovsky, Rich models for steganalysis of digital images, IEEE Trans. Inf. Forensics Secur. 7 (3) (2012) 868–882.
[9] P. Wang, F. Liu, C.F. Yang, Towards feature representation for steganalysis of spatial steganography, Signal Process. 169 (2020) 107422.
[10] Z. Jin, G. Feng, Y. Ren, X. Zhang, Feature extraction optimization of JPEG steganalysis based on residual images, Signal Process. 170 (2020) 107455.
[11] T. Filler, J. Fridrich, Gibbs construction in steganography, IEEE Trans. Inf. Forensics Secur. 5 (4) (2010) 705–720, http://dx.doi.org/10.1109/TIFS.2010.2077629.
[12] V. Holub, J. Fridrich, Designing steganographic distortion using directional filters, in: 2012 IEEE International Workshop on Information Forensics and Security (WIFS), 2012, pp. 234–239, http://dx.doi.org/10.1109/WIFS.2012.6412655.

[13] V. Holub, J. Fridrich, T. Denemark, Universal distortion function for steganography in an arbitrary domain, EURASIP J. Inf. Secur. 2014 (1) (2014) 1–13.
[14] M. Hussain, A.W.A. Wahab, Y.I.B. Idris, A.T.S. Ho, K.-H. Jung, Image steganography in spatial domain: A survey, Signal Process., Image Commun. 65 (2018) 46–66.
[15] B. Li, S. Tan, M. Wang, J. Huang, Investigation on cost assignment in spatial image steganography, IEEE Trans. Inf. Forensics Secur. 9 (8) (2014) 1264–1277, http://dx.doi.org/10.1109/TIFS.2014.2326954.
[16] L. Guo, J. Ni, W. Su, C. Tang, Y. Shi, Using statistical image model for JPEG steganography: Uniform embedding revisited, IEEE Trans. Inf. Forensics Secur. 10 (12) (2015) 2669–2680, http://dx.doi.org/10.1109/TIFS.2015.2473815.
[17] W. Su, J. Ni, X. Li, Y. Shi, A new distortion function design for JPEG steganography using the generalized uniform embedding strategy, IEEE Trans. Circuits Syst. Video Technol. 28 (12) (2018) 3545–3549, http://dx.doi.org/10.1109/TCSVT.2018.2865537.
[18] J. Fridrich, J. Kodovsky, Multivariate gaussian model for designing additive distortion for steganography, in: 2013 IEEE International Conference on Acoustics, Speech and Signal Processing, 2013, pp. 2949–2953, http://dx.doi.org/10.1109/ICASSP.2013.6638198.
[19] V. Sedighi, R. Cogranne, J. Fridrich, Content-adaptive steganography by minimizing statistical detectability, IEEE Trans. Inf. Forensics Secur. 11 (2) (2016) 221–234, http://dx.doi.org/10.1109/TIFS.2015.2486744.
[20] Z. Wang, Z. Qian, X. Zhang, M. Yang, D. Ye, On improving distortion functions for JPEG steganography, IEEE Access 6 (2018) 74917–74930, http://dx.doi.org/10.1109/ACCESS.2018.2884198.
[21] W. Zhou, W. Zhang, N. Yu, A new rule for cost reassignment in adaptive steganography, IEEE Trans. Inf. Forensics Secur. 12 (11) (2017) 2654–2667, http://dx.doi.org/10.1109/TIFS.2017.2718480.
[22] W. Zhou, W. Li, K. Chen, H. Zhou, W. Zhang, N. Yu, Controversial "®pixel" prior rule for JPEG adaptive steganography, IET Image Process. 13 (9) (2019) 24–33.
[23] Z. Zhao, Q. Guan, H. Zhang, X. Zhao, Improving the robustness of adaptive steganographic algorithms based on transport channel matching, IEEE Trans. Inf. Forensics Secur. 14 (7) (2019) 1843–1856, http://dx.doi.org/10.1109/TIFS.2018.2885438.
[24] Y. Zhang, X. Luo, Y. Guo, C. Qin, F. Liu, Multiple robustness enhancements for image adaptive steganography in lossy channels, IEEE Trans. Circuits Syst. Video Technol. (2019) 1, http://dx.doi.org/10.1109/TCSVT.2019.2923980.
[25] F. Li, K. Wu, C. Qin, J. Lei, Anti-compression JPEG steganography over repetitive compression networks, Signal Process. 170 (2020) 107454.
[26] W. Lu, J. Zhang, X. Zhao, W. Zhang, J. Huang, Secure robust JPEG steganography based on AutoEncoder with adaptive bch encoding, IEEE Trans. Circuits Syst. Video Technol. (2020) 1, http://dx.doi.org/10.1109/TCSVT.2020.3027843.
[27] Z. Yin, L. Ke, Robust adaptive steganography based on dither modulation and modifcation with re-compression, in: IEEE Transactions on Signal and Information Processing over Networks, 2021, p. 1, http://dx.doi.org/10.1109/TSIPN.2021.3081373.
[28] V. Sedighi, J. Fridrich, R. Cogranne, Toss that bossbase, alice!, in: IS&T, Electronic Imaging, Media Watermarking, Security, and Forensics, 2016, pp. 14–18.
[29] T. Pevny, A.D. Ker, Exploring non-additive distortion in steganography, in: Proceedings of the 6th ACM Workshop on Information Hiding and Multimedia Security, 2018, pp. 109–114, http://dx.doi.org/10.1145/3206004.3206015.
[30] V. Holub, J. Fridrich, Low-complexity features for JPEG steganalysis using undecimated DCT, IEEE Trans. Inf. Forensics Secur. 10 (2) (2015) 219–228.
[31] X. Song, F. Liu, Z. Zhang, C. Yang, X. Luo, L. Chen, 2D Gabor filters-based steganalysis of content-adaptive JPEG steganography, Multimedia Tools Appl. 76 (24) (2017) 26391–26419.
[32] C. Xia, Q. Guan, X. Zhao, Z. Xu, Y. Ma, Improving GFR steganalysis features by using Gabor symmetry and weighted histograms, in: Proc. 5th ACM Workshop Inf. Hiding Multimedia Security, Philadelphia, PA, USA, 2017, pp. 55–66.
[33] V. Holub, J. Fridrich, Random projections of residuals for digital image steganalysis, IEEE Trans. Inf. Forensics Secur. 8 (12) (2013) 1996–2006.
[34] P. Bas, T. Filler, T. Pevný, 'Break our steganographic system': The ins and outs of organizing BOSS, in: Proc. 13th Int. Workshop Inf. Hiding, Prague, Czech Republic, pp. 59–70.
[35] J. Kodovský, J. Fridrich, V. Holub, Ensemble classifiers for steganalysis of digital media, IEEE Trans. Inf. Forensics Secur. 7 (2) (2012) 432–444.
[36] R. Cogranne, Q. Giboulot, P. Bas, ALASKA#2: Challenging academic research on steganalysis with realistic images, in: 2020 IEEE International Workshop on Information Forensics and Security (WIFS), 2020, pp. 1–5, http://dx.doi.org/10.1109/WIFS49906.2020.9360896.
[37] J. Kodovsky, J. Fridrich, Effect of image downsampling on steganographic security, IEEE Trans. Inf. Forensics Secur. 9 (5) (2014) 752–762, http://dx.doi.org/10.1109/TIFS.2014.2309054.
[38] R. Cogranne, V. Sedighi, J. Fridrich, T. Pevny, Is ensemble classifier needed for steganalysis in high-dimensional feature spaces? in: 2015 IEEE International Workshop on Information Forensics and Security (WIFS), 2015, pp. 1–6, http://dx.doi.org/10.1109/WIFS.2015.7368597.
[39] M. Boroumand, M. Chen, J. Fridrich, Deep residual network for steganalysis of digital images, IEEE Trans. Inf. Forensics Secur. 14 (5) (2019) 1181–1193, http://dx.doi.org/10.1109/TIFS.2018.2871749.
[40] Y. Yousfi, J. Butora, E. Khvedchenya, J. Fridrich, ImageNet pre-trained CNNs for JPEG steganalysis, in: 2020 IEEE International Workshop on Information Forensics and Security (WIFS), 2020, pp. 1–6, http://dx.doi.org/10.1109/WIFS49906.2020.9360897.
[41] R. Cogranne, Q. Giboulot, P. Bas, Steganography by minimizing statistical detectability: The cases of JPEG and color images, in: Proceedings of the 2020 ACM Workshop on Information Hiding and Multimedia Security, Association for Computing Machinery, New York, NY, USA, 2020, pp. 161–167.